

Global and regional modeling of clouds and aerosols in the marine boundary layer during VOCALS: The VOCA Intercomparison

Matthew C. Wyant¹, Christopher S. Bretherton¹, Robert Wood¹, Gregory R. Carmichael², Antony Clarke³, Jerome Fast⁴, Rhea George¹, William I. Gustafson Jr.⁴, Cécile Hannay⁵, Axel Lauer^{6*}, Yanluan Lin^{7**}, Jean-Jacques Morcrette⁸, Jane Mulcahy⁹, Pablo E. Saide², Scott N. Spak², Qing Yang⁴

¹Department of Atmospheric Sciences, University of Washington, Seattle, WA, USA

²Center for Global and Regional Environmental Research (CGRER), University of Iowa, Iowa City, IA, USA

³School of Ocean and Earth Science Technology (SOEST), University of Hawaii at Manoa, Honolulu, HI, USA

⁴Pacific Northwest National Laboratory, Richland, WA, USA

⁵National Center for Atmospheric Research, Boulder, CO, USA

⁶International Pacific Research Center, University of Hawaii at Manoa, Honolulu, HI

⁷Geophysical Fluid Dynamics Laboratory, Princeton, NJ, USA

⁸European Center for Medium-Range Forecasts, Shinfield Park, Reading, UK

⁹Met Office, Exeter, UK

* Now at: Institute for Advanced Sustainability Studies, Potsdam, Germany

** Now at: Ministry of Education Key Laboratory for Earth System Modeling, Center of Earth System Sciences, Tsinghua University, Beijing, China

Second Revision for ACP

November 4, 2014

Correspondence to: Matthew Wyant (mwyant@atmos.washington.edu)

1 **Abstract**

2
3 A diverse collection of models are used to simulate the marine boundary layer in the
4 Southeast Pacific region during the period of the October-November 2008 VOCALS REx
5 field campaign. Regional models simulate the period continuously in boundary-forced
6 free-running mode, while global forecast models and GCMs are run in forecast mode.
7 The models are compared to extensive observations along a line at 20°S extending
8 westward from the South American coast. Most of the models simulate cloud and
9 aerosol characteristics and gradients across the region that are recognizably similar to
10 observations, despite the complex interaction of processes involved in the problem, many
11 of which are parameterized or poorly resolved. Some models simulate the regional low
12 cloud cover well, though many models underestimate MBL depth near the coast. Most
13 models qualitatively simulate the observed offshore gradients of SO₂, sulfate aerosol,
14 CCN concentration in the MBL as well as differences in concentration between the MBL
15 and the free troposphere. Most models also qualitatively capture the decrease in cloud
16 droplet number away from the coast. However, there are large quantitative inter-model
17 differences in both means and gradients of these quantities. Many models are able to
18 represent episodic offshore increases in cloud droplet number and aerosol concentrations
19 associated with periods of offshore flow. Most models underestimate CCN (at 0.1%
20 supersaturation) in the MBL and free troposphere. The GCMs also have difficulty
21 simulating coastal gradients in CCN and cloud droplet number concentration near the
22 coast. The overall performance of the models demonstrates their potential utility in
23 simulating aerosol-cloud interactions in the MBL, though quantitative estimation of

24 aerosol-cloud interactions and aerosol indirect effects of MBL clouds with these models
25 remains uncertain.

26

27

28

29 **1. Introduction**

30

31 The Southeast Pacific (SEP) region has an unusually extensive and persistent low-cloud
32 cover supported by relatively low sea surface temperatures (SSTs) due to coastal
33 upwelling, strong subsidence, and high static stability in the lower troposphere. There are
34 typically strong east-west aerosol gradients in this marine boundary layer (MBL) between
35 relatively pristine conditions in air masses advecting from the South Pacific Ocean and
36 more polluted air near the west coast of South America (e.g. Bretherton et al. 2010, Allen
37 et al. 2011). Anthropogenic aerosol and aerosol precursor emissions from industrial,
38 agricultural, and transportation sources are incorporated into the MBL directly or through
39 intermittent free-tropospheric flow over the ocean and subsequent entrainment into the
40 MBL (e.g. Clarke et al. 2010, George et al. 2013).

41

42 The persistent clouds and aerosol gradients make the SEP an attractive test bed for
43 evaluating how well modern forecasting and climate models can simulate aerosol-cloud
44 interactions, a key uncertainty in understanding the 20th century climate record and an
45 important issue for climate projection (IPCC 2007). This was a central motivation for the
46 Variability of the American Monsoon Systems (VAMOS) Ocean-Cloud-Atmosphere-
47 Land Study Regional Experiment (VOCALS-REx) field campaign, which took place in
48 the SEP region during October and November 2008 (Wood et al. 2011a).

49

50 In addition to the features given above, many factors coincide to make the SEP unique in
51 terms of its persistent cloud deck. The subsiding air above the MBL is also exceptionally
52 dry, enhancing radiative cooling of the MBL clouds. The temperature inversion at the top
53 of the MBL in the region is extremely strong, commonly exceeding 12 K during the
54 austral spring. Another prominent feature influencing regional meteorology and climate
55 is the Andes mountain range, which forms a long, mostly north-south barrier to east-west
56 flow in the MBL (Richter and Mechoso, 2006). This feature together with the strong
57 inversion controls the circulations that affect aerosol and chemical transport pathways.
58 The meteorology of the region in the austral spring season is dominated by a subtropical
59 anticyclone. The flow in the MBL (Fig. 1) is typically southerly near the coast turning
60 southeasterly away from the coast. There is a climatological advection of coastal air to
61 the northwest, away from the coast and towards higher SSTs. The MBL deepens as it is
62 advected offshore over higher SSTs. This flow pattern also carries aerosols from coastal
63 anthropogenic and natural sources offshore. Aerosols generated farther inland and/or
64 lofted upwards may also enter the SEP MBL through advection offshore at higher levels
65 and entrainment into the MBL-top (Saide et al., 2012, George et al. 2013).

66

67 Skillful simulation of aerosol-cloud interaction in the MBL requires a realistic
68 representation of other boundary layer cloud processes in models. However, the accurate
69 simulation of boundary layer clouds such as stratocumulus and trade cumulus is a long-
70 standing challenge in climate and weather forecast modeling. The Pre-VOCALS
71 Assessment (PreVOCA, Wyant et al. 2010) was designed to document and evaluate a

72 wide range of models in the SEP region and to provide a benchmark for future model
73 comparisons to VOCALS-REx observations. PreVOCA examined simulations of the
74 VOCALS-REx study region for October 2006 using a collection of 15 regional and
75 global models and compared them with satellite data and ship-based climatologies
76 available before VOCALS-REx. Most of these models had no explicit representation of
77 aerosols. Many of the models produced serious biases in the time-mean geographic
78 variability of low cloud in this region. In most models, the simulated MBL was too
79 shallow near the coast. Nevertheless, a subset of models simulated the space-time
80 distribution of cloud cover and thickness quite well.

81

82 The extensive in-situ sampling during VOCALS-REx, especially from aircraft, provides
83 more detailed and direct comparisons for models than were available for PreVOCA.
84 These include comparisons of aerosol and chemical constituents (Bretherton et al. 2010;
85 Allen et al. 2011) as well as MBL vertical structure and precipitation. This dataset is
86 uniquely suited to testing simulations of MBL cloud, aerosols, and their interactions. The
87 VOCALS Assessment (VOCA) was organized to capitalize on this opportunity.
88 Participating models simulated the SEP during the month of VOCALS-REx when aircraft
89 observations were being made. Sixteen modeling groups submitted simulations from
90 global climate models, global operational forecast models, and regional models. In this
91 study we focus on the subset of 9 VOCA models that have some representation of
92 aerosols and their effects on clouds.

93

94 There are a number of prior modeling studies of the SEP during VOCALS REx. Abel et
95 al. (2010) evaluate the simulations of cloud cover, MBL depth, and precipitation over the
96 entire REx period as well as over the diurnal cycle using a limited area model (LAM)
97 configuration of the UK Met Office Unified Model. Q. Yang et al. (2011) compare their
98 WRF-Chem simulations for VOCA with observations and find that their simulations with
99 interactive aerosols perform better than those with a passive treatment of aerosols. Their
100 follow-up modeling study (Yang et al., 2012) quantified the relative impacts of regional
101 anthropogenic and oceanic emissions on aerosol properties, cloud macro- and
102 microphysics, and cloud radiative forcing over the SEP during VOCALS, and reported a
103 large feedback of aerosol concentration on precipitation and aerosol lifetime over the
104 clean ocean environment. Saide et al. (2012), using a different configuration of WRF-
105 Chem, compare their VOCA simulations with observations over the entire study period
106 as well as over shorter episodes. They also find that aerosol indirect effects play an
107 important role in their simulations, and that their treatment of aerosol wet deposition has
108 a strong impact on their results. George et al. (2013) used WRF-Chem in a similar
109 configuration to their runs presented here to study multi-day ‘hook’ events, where
110 polluted continental air is carried offshore and influences stratocumulus clouds via
111 aerosol indirect effects.

112

113 This paper addresses several questions: Can the models represent the geographical
114 contrasts in cloud microphysical properties in the SEP? How well do the geographical
115 and vertical concentrations of aerosols agree? How well do the models represent the

116 impacts of these aerosols in the clouds? What problems are common to many models?
117 Do these observations provide a good benchmark for aerosol/cloud interaction?
118 We will describe the setup of VOCA in Section 2. Section 3 compares the model results
119 with each other and with observations. The results of the comparison will be discussed in
120 Section 4 and conclusions presented in Section 5. Detailed descriptions of the models
121 used are given in an Appendix.

122

123

124 **2. Case Setup**

125 VOCA covers the time interval from 0 UTC 15 Oct 2008 through 0 UTC 16 November
126 2008, the period of VOCALS REx intensive airborne observations. The outer study
127 region for VOCA is shown in Fig. 1. The inner domain outlined in black extends from
128 12°S to 35°S and 68.5°W to 88°W, which includes the region of most of the REx research
129 flights including the large set of flights along 20°S from the coast to 85°W. Simulation
130 output data in the outer and inner region were horizontally averaged to a 1° x 1° grid and
131 0.25° x 0.25° grid, respectively, by the modeling groups. The models were not required to
132 match their simulation domains to the outer and inner domains, or to necessarily include
133 the outer study domain; the regional models in this comparison did not cover this outer
134 study domain due to computational demands. Each model submitted data on its native
135 vertical levels to preserve vertical structure for analysis. The data were submitted with 3-
136 hour time resolution, with some data fields averaged over 3-hour intervals, and other
137 fields provided at 3-hour snapshots. The experiment specification can be found at
138 http://www.atmos.washington.edu/~mwyant/vocals/model/VOCA_Model_Spec.htm.

139

140 A diverse group of models are represented in this study. They include global general
141 circulation models (GCMs): the National Center for Atmospheric Research (NCAR)
142 Community Atmosphere Model versions 4 and 5, (CAM4 and CAM5, respectively) and
143 the NOAA Geophysical Fluid Dynamics Atmospheric Model 3 (GFDL AM3).
144 Simulations using global weather forecast models were provided by the European Centre
145 for Medium-Range Weather Forecasts (ECMWF) and the UK Met Office (UKMO).
146 Regional simulations using the Weather Research and Forecasting model coupled with
147 Chemistry (WRF-Chem) were submitted independently by research groups from
148 University of Iowa, Pacific Northwest National Laboratory, and the University of
149 Washington (hereafter labeled IOWA, PNNL, and UW, respectively). Another regional
150 simulation included in this study was produced by the International Pacific Research
151 Center (IPRC) with their Regional Atmospheric Model (iRAM). Detailed descriptions of
152 these models are given in the Appendix.

153

154 Table 1 shows a list of the VOCA simulations analyzed in this study and many of their
155 important parameters and characteristics. All of the listed global models were run in
156 forecast mode, i.e., as a series of short simulations initialized at subsequent times from
157 externally specified conditions. This initialization constrains the large-scale environment
158 while still allowing the model to develop internally consistent representations of cloud
159 and boundary layer structure. Forecast-mode has proven to be a good framework for
160 identifying climate model biases (e.g. Phillips et al. 2004, Boyle et al. 2008, Hannay et al.
161 2009). Daily forecasts were provided by the modeling groups (twice-daily for the

162 UKMO model), and for each model, data from these were stitched together to cover the
163 REx period. The global weather forecast models used a data assimilation/forecast cycle
164 that did not have a large initialization shock for boundary layer cloud, so the first forecast
165 period (which presumably has the most accurate meteorological fields) was used in our
166 study (e. g. 0-12 hours for UKMO). The global climate models were initialized from
167 ECMWF high-resolution global analyses produced for the Year of Tropical Convection
168 (YOTC), so there was a spin up period for each model to adjust to this analysis. For such
169 models, a later forecast period was chosen for analysis. The global models each utilize
170 different land emission schemes.

171

172 All of the regional models were run continuously in free-running mode, with forcing at
173 the lateral boundaries. The lateral boundary conditions for IOWA, UW, and iRAM came
174 from the NCEP global FNL analysis, and for PNNL they came from NCEP's Global
175 Forecast System (GFS) analyses. A regional emissions inventory of natural and man-
176 made emissions over land during the VOCALS REx period was developed at University
177 of Iowa. This inventory is described by Mena-Carrasco et al. (2012) and available at
178 http://bio.cgrer.uiowa.edu/VOCA_emis/. It includes emissions from anthropogenic
179 sources and large nearby volcanoes, but not biogenic or biomass burning emissions. All
180 of the WRF-Chem regional models incorporated these emissions in their simulations, but
181 none of the other participating models use these emissions. Parameterizations for fluxes
182 of sea-salt and dimethyl sulfide (DMS) from the sea-surface were provided in the VOCA
183 specification but not required for participants. The specified coarse and fine mode sea-
184 salt emissions are based on Gong et al. (1997) and Monahan et al. (1986), while ultrafine

185 emissions follow Clarke et al. (2006). The specification uses a simplified version of
186 Nightingale et al. (2000) with a geographically uniform ocean surface DMS
187 concentration of 2.8 nmol l^{-1} . Choice of emission parameterizations for any other aerosol
188 types, such as dust, was left up to the participants. For regional models, the Model for
189 Ozone and Related chemical Tracers version 4 (MOZART-4; Emmons et al. 2010) global
190 model provided initial and lateral boundary conditions of aerosol and chemical species
191 concentrations.

192

193 The models represent aerosol size and mass to varying degrees of precision and
194 complexity. The IPRC model uses climatologically prescribed aerosol mass and size
195 distributions and permits aerosols to affect clouds, and so surface aerosol emissions are
196 not represented. The rest of the models use prognostic aerosol schemes – either they
197 specify a small number of size modes (CAM5, GFDL, UW), or use sectional schemes
198 with explicit aerosol size bins (PNNL, ECMWF, UKMO, IOWA). For models with
199 aerosol-cloud feedbacks, a fraction of the aerosols can become activated and become
200 cloud-droplet nuclei. In this way, aerosol number concentration can affect cloud-droplet
201 number concentration (N_d). N_d in turn affects drizzle formation and cloud reflectivity.
202 Cloud and precipitation scavenging reduces concentrations of both activated and
203 unactivated aerosols in the MBL.

204

205 In this study, we rely heavily on in-situ aircraft observations along 20°S and between
206 70°W , at the Chilean coast, and 85°W , at the Improved Meteorology (IMET) moored
207 research buoy situated about 1500 km offshore. Throughout VOCALS REx, several

208 aircraft, primarily the NSF C-130 and UK BAe146, regularly performed research flights
209 in and above the MBL along this line (Bretherton et al. 2010; Allen et al. 2011). A
210 common flight pattern included a sequence of 60-km level legs, one 150-300 m above the
211 inversion, one in the middle of the cloud layer or, in the absence of clouds, just below the
212 inversion base, and one in the lower MBL at 150m height. This pattern was repeated
213 multiple times along the 20°S segment. Data from 23 flights are distributed fairly evenly
214 throughout the 15 October to 16 November period and fairly evenly over the diurnal
215 cycle. Almost all C-130 and BAe146 flights sampled out to 80°W, while 4 C-130 flights
216 sampled the entire segment out to 85°W. Bretherton et al. (2010) and Allen et al. (2011)
217 provided a thorough description of the flights and findings from this collection of flight
218 data and other supporting observational data. Following those studies, we frequently sort
219 aircraft leg-mean values into 5°- or 2.5°- longitude bins before further averaging in order
220 to reduce sampling noise and facilitate comparisons with the models. The 25th- and 75th -
221 percentile values of these leg-mean values are plotted in the figures as error bars and
222 provide an estimate of the temporal and geographic variability in sampling. The actual
223 measurement errors of the means should be much smaller than these ranges.

224

225 **3. Results**

226

227 **3.1 Time-mean cloud macrophysics and precipitation**

228 We begin by comparing simulated low-cloud fraction near 1530 UTC (approximately
229 10:30am local time) averaged over the one-month REx period (Fig. 2) with satellite cloud
230 fraction from the Moderate Resolution Imaging Spectrometer (MODIS) Terra daytime

231 overpass (also approximately 10:30am local time). Note that the MODIS cloud fraction
232 includes all clouds, not just low clouds, though low clouds strongly dominate the cloud
233 fraction climatology. As in PreVOCA, many models have difficulty in simulating the
234 geographic distribution of low-cloud fraction as compared with MODIS. The models'
235 patterns of low-cloud cover are quite diverse. The PNNL, UW WRF, IOWA, and
236 ECMWF models agree well with MODIS in the northeast part of the inner study region.
237 In the southwest part of the region, PNNL and UW WRF have too little low cloud, while
238 IOWA and ECMWF models have too much. In the southern half of the inner study region
239 the CAM4 and CAM5, GFDL, UKMO, and IPRC models have too little low cloud in the
240 southern part of the study region. While CAM5, with better vertical resolution, appears to
241 be an improvement on CAM4 in the study region, the CAM5 low cloud fraction does not
242 agree any better with MODIS than CAM4 in the outer region, despite better vertical
243 resolution. The GFDL model also has too few low clouds near the coast. Along 20°S in
244 the inner study region, the GFDL and UKMO models both significantly underestimate
245 cloud fraction compared with MODIS.

246

247 Figure 3 compares the simulated liquid water path (LWP) along 20°S with mean C-130
248 airborne microwave radiometer observations (Zuidema et al. 2012) during VOCALS and
249 with mean satellite observations from the Advanced Microwave Scanning Radiometer-
250 EOS (AMSR-E) on NASA's AQUA satellite. The AMSR-E values include both daytime
251 and nighttime passes. Also plotted is a 2001-2008 October-November climatology of
252 LWP along 20°S from the ship-based radiometer measurements of the Ron Brown from
253 2001-2008 (de Szoek et al. 2012). Both satellite and aircraft measure a mean increase in

254 LWP moving westward (offshore) from the near-coastal MBL and then a more constant
255 LWP further offshore, while in the Ron Brown climatology the LWP increases further
256 offshore. The LWP along 20°S varies considerably between models. Most of the models
257 underpredict mean LWP over most of the 20°S profile, while a few models overpredict
258 LWP nearer to the coast. Most models are within a factor of two of the observed means.

259

260 Figure 4 shows the mean cloud-top height for all the models at 20°S compared with the
261 mean of C-130 aircraft leg-mean cloud-top values and a Ron Brown 2001-2008 cloud-top
262 height climatology (de Szoeke et al. 2012). All of the models underestimate cloud-top
263 height, with negative biases from 100 m to 700 m and particularly large biases near the
264 coast. Similar underestimates of MBL depth near the coast were common in PreVOCA
265 (Wyant et al. 2010). The WRF models compare better with aircraft observations than the
266 other models along 20°S with negative biases less than 200 m in each longitude bin. The
267 relative performance of various models is consistent with the study of Wang et al. (2011),
268 which argues that both horizontal and vertical model resolution appear to be important in
269 predicting MBL height. Most models match the observed westward increase of the cloud-
270 top height. The main exception is the IPRC model in which cloud-top height rises too
271 rapidly to the west, related to its strong negative bias in cloud-top height near the coast.

272

273 The general deepening of the boundary layer to the west along 20°S is also evident in Fig.
274 5, a comparison of the cloud fraction profiles at 75°W and 85°W. Also shown are profiles
275 of cloud fraction from cloud-base and cloud-top measurements taken on Ronald H Brown
276 cruises during VOCALS REx along 20°S, which were sorted into measurements west of

277 80°W and east of 80°W (Burleyson et al. 2013). The periods of these measurements (25
278 October to 2 November 2008 and 10 November to 2 December 2008) only partly overlap
279 with the VOCA study period. The modeled and observed vertical extent of cloud fraction
280 is broader to the west, consistent with a more decoupled vertical structure associated with
281 cumuliform convection in the MBL and/or stronger time variations in inversion height.
282 The overall distribution of modeled cloud heights is consistent with the cloud-top height
283 comparison of Fig. 4. Models with fine vertical resolution in the MBL and lower
284 troposphere (PNNL, IOWA) are able to represent the Gaussian shape of the
285 measurements where models with coarser resolution show less smooth profiles. The
286 height of peak cloud fraction in Fig. 5 is lower in almost all models than the
287 corresponding observed peak, but in this case the comparison could be influenced by the
288 mismatch of observation times and locations with those used for model averaging.
289
290 Mean surface precipitation rates in the region are generally very small, much less than 1
291 mm day⁻¹ (Bretherton et al. 2010, Wood et al. 2012, Rapp et al. 2013), but precipitation
292 processes still play an important role in the MBL. Drizzle redistributes moisture
293 downward and stabilizes the MBL through evaporation. In this environment cloud and
294 precipitation scavenging is the dominant removal process of sub-micron aerosols.
295 Precipitation feedbacks also may play a central role in the formation and maintenance of
296 pockets of open cells (POCs), which are common features of the regional marine
297 stratocumulus (Bretherton et al. 2004; Wood et al. 2008; Wood et al. 2011b, Ovchinnikov
298 et al. 2013).
299

300 Figure 6 compares time-mean modeled surface precipitation, time-mean aircraft
301 observations, and a 2006-2010 satellite precipitation climatology (Rapp et al. 2013) from
302 the NASA CloudSat 2C-RAIN-PROFILE product that includes both daytime and
303 nighttime passes. The aircraft measurements were made at about 150 m above the
304 surface using the Particle Measuring Systems 2D-C instrument. Both observational
305 datasets are subject to considerable uncertainty that is associated with both the
306 measurement technique and the representativeness of the sampling. The models tend to
307 produce more surface precipitation than suggested by CloudSat retrievals. Near the coast
308 limited CloudSat observations suggest miniscule precipitation rates. Some models agree
309 well with this (CAM5, UKMO, PNNL, and IOWA), while the other models predict more
310 significant precipitation rates. Offshore, all models are within an order of magnitude of
311 observed values.

312

313

314 **3.2. Time-mean aerosol and chemical properties**

315 We next compare the simulated aerosol and chemical properties along 20°S with the REx
316 observations. We focus on aerosols that directly impact MBL clouds in this region
317 through their capacity to act as cloud condensation nuclei (CCN). We compare modeled
318 and C-130 measured CCN number concentration at 0.1% supersaturation in the free
319 troposphere above the inversion (FT, Fig. 7, top-left panel) and at 150 m height (Fig. 7,
320 bottom-left panel). The specification of 0.1% supersaturation was in retrospect
321 suboptimal for the intercomparison, since it is somewhat lower than the 0.2-0.4%
322 maximum supersaturation expected during the nucleation of cloud droplets given typical

323 MBL updraft strengths and aerosol size spectra (Martin et al. 1994, Snider et al. 2003,
324 Hudson et al. 2010). This may lead to an underestimate of the actual number
325 concentration of aerosol that nucleate cloud droplets. However, given other large
326 parameterization uncertainties, this statistic is still a useful comparison between models
327 and observations. In all figures, FT aircraft observations are sampled above cloud and
328 between 1700 m and 3200 m, while model FT means are computed from the inversion
329 height to 3200 m, following Allen et al. (2011). At 150 m, with the exception of the
330 UKMO model, all of the models have mean CCN concentrations in the MBL and FT that
331 are about half as large as observed or even less, both near shore and offshore. WRF-
332 Chem models using the MOSAIC sectional aerosol scheme and the Abdul-Razzak and
333 Ghan (2002) activation scheme (PNNL and IOWA) have significant concentrations of
334 accumulation mode aerosol that do not activate at this low supersaturation, and aerosol
335 concentrations show much better agreement with VOCALS observations in the MBL
336 when these accumulation mode aerosols are considered (Q. Yang et al. 2011, Saide et al.
337 2012). East of 80°W, the UKMO model has excessive CCN concentrations at all
338 longitudes, reaching a peak of 1700 cm⁻³ at 74°W. In the FT the model concentrations of
339 the other models are also lower than observed. Most of the models have some semblance
340 of the offshore CCN gradient seen in the observations.

341

342 Observational studies in the VOCALS region confirm that sulfate aerosol is the most
343 important aerosol for nucleating cloud droplets (e.g. Twohy et al. 2013). While number
344 concentration of accumulation-mode sulfate aerosol may be more directly relevant to
345 cloud-aerosol interaction than sulfate mass, only the latter quantity was archived by most

346 models and will be compared with observations. In the right panels of Fig. 7, modeled
347 total mean sulfate aerosol mass is compared with C-130 and BAe-146 Aerosol Mass
348 Spectrometer (AMS) sulfate aerosol mass from 0.05 μm - 0.5 μm . Here the model MBL
349 values are vertical means with the MBL thickness determined as for Fig. 4. In both the
350 MBL and the FT, the models all have significant offshore gradients of sulfate aerosol
351 comparable to the observations, consistent with a continental source. The models differ
352 considerably in sulfate mass, especially in the MBL, but the majority of models tend to
353 have less FT and more MBL sulfate aerosol mass than the AMS values. It should be
354 noted that the AMS values represent a lower bound on actual sulfate mass, as there can
355 be significant mass contained in aerosols larger than 0.5 μm diameter (e.g. Q. Yang et al.
356 2011). In the MBL, the models are more skillful representing sulfate mass than CCN
357 number concentration, with most models within a factor of two of the observed means.

358

359 Two important atmospheric precursors to sulfate aerosol are dimethyl sulfide (DMS) and
360 SO_2 . DMS is the only local source of (non-sea-salt) sulfate aerosol in remote ocean
361 regions. Figure 8 shows a comparison of mean MBL DMS concentration of most of the
362 models with aircraft observations. Also shown are mean near-surface atmospheric DMS
363 observations from the Ron Brown during VOCALS-REx (M. Yang et al. 2011). The
364 timing of these observations only partly overlaps the VOCA simulation period, as was the
365 case with the Ron Brown cloud-fraction profiles shown above. The DMS concentrations
366 vary widely across models but are generally higher than the aircraft observed values for
367 some models. The Ron Brown observed near-surface values are notably higher than
368 aircraft values, which can be partially explained by the general decrease of DMS

369 concentration with height in the MBL (e.g. M. Yang et al. 2011). The specified ocean
370 surface DMS concentration is a spatially uniform 2.8 nM for the WRF models (as given
371 in the VOCA specification). While it may differ somewhat in the other models, the
372 differences are very unlikely to account for the wide variation between models.
373 Differences in mean surface wind speed and advection patterns also can't account for
374 DMS differences. Over most of the inner study region, the interquartile range across
375 models of mean model surface wind speeds less than 2 m s^{-1} and the interquartile range of
376 both meridional and zonal 10-m winds is less than 1.5 m s^{-1} . Furthermore, the inter-model
377 differences in upstream mean model wind speed appear to be uncorrelated with model
378 mean DMS concentrations. The large differences in MBL DMS concentration are most
379 likely due to differences in surface flux parameterizations or differences in model
380 chemistry. Both models and observations agree that MBL DMS concentrations are larger
381 offshore than near the coast, possibly due to the much higher wind speed offshore. PNNL
382 WRF-Chem significantly overestimates the DMS concentration in the atmosphere, and
383 detailed investigation by Q. Yang et al. (2011) partially attributes this to overestimation
384 of the DMS ocean-to-atmosphere transfer velocity. However, the PNNL WRF mean wind
385 speeds along 20°S are very similar to UW WRF and GFDL, whose mean 20°S MBL
386 DMS concentrations are much lower.

387

388 Both modeled and observed profiles of gas phase SO_2 along 20°S (Fig. 9) in the MBL and
389 the FT show even sharper gradients near the coast than for SO_4 aerosol mass. There is
390 abundant SO_2 near shore due to continental anthropogenic and natural sources, but the
391 SO_2 is low offshore compared with aircraft values in both the MBL and the FT. The

392 abundance of modeled SO₂ in the near shore and the strong modeled offshore sulfate
393 gradient in the MBL suggests the models are producing most of their MBL sulfate
394 aerosol east of 80°W via oxidation of SO₂. This mechanism is generally consistent with
395 findings of M. Yang et al. (2011) based on observed offshore SO₂ and SO₄ budgets in
396 VOCALS-REx. The offshore model differences in the FT SO₂ are likely due to
397 differences in background SO₂ in the models. The only model that matches the observed
398 values (IOWA) has specified minimum thresholds for its SO₂ boundary conditions (Saide
399 et al. 2012). For the offshore MBL, most models, including the three WRF-Chem
400 simulations, underestimate SO₂, which has been hypothesized to be due to SO₂ to SO₄
401 aqueous reaction rates that are too fast (Saide et al. 2012). However the aircraft
402 concentrations in the remote MBL are suspiciously high, as there were almost no
403 measured SO₂ concentrations below 10 pptv during VOCALS flights, even during
404 nighttime.

405

406 Another significant potential source of aerosol mass and number in the MBL, especially
407 in the remote regions, is sea-spray aerosol (SSA) generated by bubble bursting. The SSA
408 mass in the MBL is thought to be dominated by the largest 10% of the total number
409 concentration, with dry diameters exceeding 1 μm while number concentrations and
410 contributions to CCN are dominated by the smaller sizes (Clarke et al. 2006). Here we
411 compare modeled SSA (dry) mass mixing ratio with C-130 aircraft observed estimates
412 (Fig. 10). These estimates from Blot et al. (2013) are based on data from particle counters
413 and a Giant Nuclei Impactor and consider SSA particle sizes from about 0.04μm to tens
414 of micrometers. The observed trend to lower values west of 80°W has been attributed to

415 more effective removal by drizzle in spite of higher winds and SSA production (Blot et
416 al. 2013). There is a substantial range in simulated SSA mass, with most models
417 exceeding the observed mean values. However, the WRF-Chem models and the GFDL
418 models are generally close to the aircraft interquartile ranges. The inter-model range of
419 mean surface wind speeds in the study region is small (as noted above) and uncorrelated
420 with SSA mass. Some models have upper size limits due to the sectional approach used
421 (e.g. the MOSIAC model used in the PNNL WRF and IOWA WRF has a 10 μm cutoff)
422 limiting their total SSA mass somewhat. The expected mass contribution of aerosols
423 smaller than 0.04 μm is negligible.

424

425 We next compare in Fig. 11 modeled cloud droplet number concentration (N_d) with
426 aircraft-observed N_d and MODIS N_d retrieved using the method of George and Wood
427 (2010). Five of the seven plotted models underestimate droplet concentration compared
428 with aircraft and MODIS observations, especially near the coast. (Note that model N_d is
429 computed only in grid-cells where 3-hour cloud liquid water exceeds 0.1 g kg^{-1} .) The
430 general under-prediction of N_d is consistent with the under-prediction of the larger CCN
431 by all models shown above. However, other model parameterizations, especially the
432 representation of local updraft velocity and its role in droplet activation, can also play a
433 large role in ultimately determining N_d . The majority of models do show the expected
434 gradient in N_d moving away from the coast. The high UKMO concentrations near the
435 coast are consistent with the extremely high CCN concentrations in that model. But the
436 CAM5 and GFDL models have droplet concentrations near the coast that are not
437 appreciably higher than farther offshore.

438

439 A strong connection between CCN and N_d in most models is evident in Figs. 12 and 13,
440 which show their time evolution along 20°S over the duration of the experiment. CCN
441 concentrations at 150 m are shown. Daily MODIS N_d from Bretherton et al. 2010 is also
442 plotted during periods when local MODIS cloud fraction was greater than 80%, which
443 are favorable for a reliable satellite-based N_d estimate. For some models, the LWC
444 threshold for reporting simulated N_d often filters out results, especially during the early
445 afternoon cloudiness minimum. Most models have higher CCN concentrations near the
446 coast at most times, with occasional excursions of high CCN air westward coincident
447 with periods of high N_d . The exceptions are the GFDL and the IPRC models. The GFDL
448 model has comparatively low liquid water concentrations, so N_d is unreported over much
449 of the experiment domain and time making it difficult to discern N_d variations. IPRC has
450 fixed aerosol concentrations which causes CCN concentrations to have minimal time
451 dependence. The other models differ considerably in the westward extent and timing of
452 high CCN and N_d excursions. Most models qualitatively agree about two periods of high
453 CCN and N_d , also observed by MODIS, one from Julian Days (JD) 291-295, and one
454 from JD315-320. The models tend to show two secondary peaks in CCN near JD302 and
455 JD310, also visible in the MODIS N_d , but the temporal variation of modeled N_d during
456 the middle of the study period is not consistent between models.

457

458 Figure 14 also illustrates the strong connection between CCN and N_d . Plotted are mean
459 values of modeled and observed CCN (0.1% supersaturation, 150m) and N_d binned by
460 longitude along 20°S. While the models vary greatly in absolute droplet number relative

461 to CCN, and in gradient of CCN and N_d offshore, most models show a near one-to-one
462 slope on the log-log plot, suggesting a nearly linear relationship between CCN and N_d .
463

464 Black carbon (BC) aerosol is a key tracer for the presence of sub-micrometer combustion
465 derived aerosol. Although it is usually only a few percent of combustion aerosol mass,
466 when BC is elevated above “clean” conditions it indicates combustion aerosol is
467 contributing directly to aerosol mass, number and CCN. Unlike CO, BC in aged
468 combustion aerosol is readily scavenged by precipitation such that ambient
469 concentrations reflect the impact of both source and removal processes. Figure 15
470 compares BC aerosol mass for several models with binned C-130 aircraft measurements
471 made with a single particle soot photometer, which measures BC aerosol of diameter
472 $0.087 - 0.4\mu\text{m}$ (Shank et al. 2012). The models’ spread in MBL concentrations is large,
473 especially near the coast, but with all models generally within one order of magnitude of
474 observed means. Despite the large biases in many models, most do show an increase in
475 black carbon concentration towards the coast in the MBL, as observed. One exception to
476 this trend is UW. This model does not include biomass burning, which explains the large
477 difference between it and the other models near land. The models generally
478 underestimate BC in the FT. The FT observations are suggestive of an offshore
479 maximum in BC that is not captured in any of the models. The spatial and temporal
480 variability in aircraft measured BC in the FT makes evaluation of the model means
481 difficult.
482

483 Two other trace gases measured during VOCALS flights are ozone and CO. Although
484 they do not interact strongly with clouds, they provide an interesting comparison with
485 models because this region is data-sparse and distant from other locations with extensive
486 in-situ measurements through the lower troposphere. These gases (especially CO) are
487 long lived; hence they are strongly determined by boundary conditions in the regional
488 models. Thus these model comparisons, especially for CO, are a stronger test for global
489 than regional models.

490

491 Ozone concentrations are compared in Fig. 16. As noted in Allen et al. (2011), mean O₃
492 concentrations measured in this region are higher in the free troposphere than in the
493 MBL, generally consistent with subsidence of higher-ozone upper-tropospheric air, and
494 the models reproduce this pattern. The PNNL WRF and IOWA WRF models match the
495 observed means fairly well. Ozone can also be produced around anthropogenic pollution
496 plumes. However, observed longitudinal gradients of O₃ are small in the boundary layer,
497 and in the FT there actually is a 25% drop in concentration near the coast; Allen et al.
498 (2011) attributed this to enhanced mixing with ozone-poor boundary-layer air, which
499 overwhelms any coastal anthropogenic source. The IOWA WRF and GFDL runs have a
500 lesser but noticeable coastal decrease in O₃; the CAM models have a slight ozone
501 increase in the MBL and no decrease in the FT, suggestive of an overly strong coastal
502 ozone source.

503

504 CO concentrations (not shown) were available only from the WRF-Chem regional
505 models and the GFDL global runs. Aircraft mean values from 75°W to 85°W were 66

506 ppbv in the MBL and 75 ppbv in the FT with weak longitudinal variation, and the model
507 means were generally within ± 10 ppbv of observed means along 20°S in both the MBL
508 and FT. Because of the relatively long lifetime of CO, differences between model means
509 are more closely tied to model boundary conditions or remote sources than to differences
510 in model physics and chemistry.

511

512

513

514 **4. Discussion**

515 In evaluating the performance of the models with respect to aerosols and clouds, it is
516 useful to group a few subsets of the models with similar characteristics. We begin with
517 two contemporary GCMs in the study, GFDL and CAM5, which have comparable
518 horizontal and vertical resolution in the MBL. Both models significantly under predict
519 LWP and inversion height along 20°S, and the GFDL model is significantly deficient in
520 cloud fraction all along 20°S, especially near the coast. Both are also deficient in CCN at
521 0.1% SS and have an apparent surplus of sulfate aerosol and SSA mass, suggesting that
522 their aerosol size distributions may be skewed towards larger sizes. Neither model
523 displays a mean offshore gradient in CCN despite having significant offshore gradients in
524 sulfate aerosol. As a result, both models underestimate observed cloud-droplet
525 concentrations, especially near the coast.

526

527 The three participating WRF-Chem models (PNNL, IOWA, and UW) show somewhat
528 differing cloud characteristics but are similar in some other respects. Since they use

529 different PBL, microphysics, chemistry, and aerosol schemes, and use different
530 horizontal and vertical grid resolutions, these models are expected to give a range of
531 results. The three models produce similar geographic patterns of low cloud but the IOWA
532 model predicts more low cloud in the southwest part of the study region than the other
533 two models, while MODIS cloud fractions have intermediate values. Along 20°S, the
534 PNNL model has the highest LWP while the IOWA and especially the UW model
535 underpredict LWP away from the coast.

536

537 On the other hand, all three models only slightly underestimate the observed MBL depth.
538 All three display prominent offshore gradients in CCN, N_d , and sulfate aerosol. All three
539 significantly underpredict CCN concentrations at 0.1% supersaturation at 20°S. However
540 the PNNL and IOWA models activate significantly more CCN at higher supersaturations
541 (not shown). The UW and PNNL simulations only slightly under-predict N_d and the
542 IOWA simulation is close to observations in the western part of the study region but over
543 predicts N_d in the eastern part.

544

545 The simulations from the two global operational forecast models, ECMWF and UKMO,
546 contrast sharply. These models are intermediate in vertical resolution between the WRF
547 models and the global climate models. The ECMWF LWP and cloud fraction agree
548 reasonably well with observations though the MBL depth is shallower than observed. The
549 UKMO model maintains realistic MBL depth, but its low cloud fraction drops to 50%-
550 60% away from the coast, somewhat less than observed, and the LWP is lower by a
551 factor of two or more than observed. Because CCN concentration and N_d are unavailable

552 from the ECMWF simulations, it is difficult to evaluate the ECMWF aerosol distribution.
553 In contrast to other models in the study, UKMO has very high concentrations of aerosol
554 and CCN, leading to very large cloud droplet concentrations compared with those
555 observed. The overestimation of sulfate aerosol was subsequently found to be due to a
556 positive bias in the emission source strength used in these simulations introduced in error
557 in the interpolation of the emissions onto the model grid.

558

559 **5. Conclusions**

560 The VOCALS-REx experiment in the SEP region provides a unique dataset of aerosols,
561 chemical constituents and marine boundary layer clouds sampled extensively by aircraft
562 and ship over a four-week period. This has provided the opportunity to compare and
563 evaluate a large group of diverse models with extended in-situ data over the longitudinal
564 transect at 20°S. Compared to the previous Pre-VOCA model assessment (Wyant et al.
565 2010) in the same region, which relied mostly on satellite measurements, the new
566 emphasis of VOCA is on aerosol-determining processes and aerosol-cloud interactions in
567 a marine stratocumulus regime. Hence our analysis in this paper has been limited to the
568 subset of nine models participating in VOCA that have some representation of aerosol
569 processes, which in some cases interacts with cloud microphysics.

570

571 Returning to the first question raised in the introduction, for many of the models,
572 accurately predicting cloud fraction, liquid water path, and precipitation remain as major
573 challenges and are critical for accurately simulating aerosol-cloud interactions. Despite
574 good simulations of the SEP pressure and wind patterns, the mean distribution of low

575 cloud in the region is still problematic and not substantively improved for many global
576 models since PreVOCA, while regional models participating in both studies (IPRC and
577 especially PNNL-WRF) exhibit better performance. Most models still tend to
578 underestimate LWP and boundary-layer depth in the study region, especially GCMs with
579 low vertical resolution, and the inter-model spread in LWP is still large. For many models
580 in VOCA, the representation of aerosol processes is a relatively new feature, and at this
581 stage of model development, we do not expect, nor generally find, that their inclusion
582 necessarily improves model simulation of cloud and boundary-layer properties relative to
583 Pre-VOCA.

584

585 Turning to our second question about how well models represent the spatial distribution
586 of aerosols, we find that along 20°S, most models were able to qualitatively represent
587 offshore and vertical gradients in aerosols and aerosol related constituents, in particular
588 the offshore reduction of aerosols in the MBL and an associated reduction in cloud-
589 droplet concentration. The models also show some skill in simulating the time-variation
590 of aerosol and cloud droplet number concentrations associated with episodic offshore
591 flow in the VOCALS study region.

592

593 Our third question asked about the fidelity of modeled aerosol-cloud interaction. Most of
594 the models in this study appear to be deficient in CCN at 0.1% supersaturation both in the
595 MBL and free troposphere. However, droplet number concentrations are unbiased in a
596 model ensemble-mean sense, indicating that for some models, significantly more
597 accumulation mode aerosol is being activated than just the CCN at 0.1% supersaturation.

598 The GCMs in this study have difficulty with properly representing offshore gradients in
599 CCN and cloud droplet number concentration near the coast. Low horizontal resolution
600 may be to blame. There is also substantial scatter in model-predicted local sources of
601 aerosol mass over the remote ocean due to DMS and SSA, even though the simulated
602 wind speeds were realistic. While the global models tended to have better DMS
603 representation than the regional models, the opposite occurred for SSA, where regional
604 models showed lower biases.

605

606 Although simulation of aerosol-cloud interactions and aerosol indirect effects in the
607 marine boundary layer clouds is a challenge, and further improvements are needed, the
608 models do capture many of the essential cloud and aerosol controlling processes in the
609 SEP. Indeed, regional models are already being successfully used to investigate aerosol
610 processes in the SEP (e.g. Q. Yang et al. 2011, Saide et al. 2012, Yang et al. 2012,
611 George et al., 2013). However, for those models with large mean biases in cloud and
612 aerosol properties, accurately simulating impacts of aerosols on clouds and vice-versa is
613 problematic. Thorough integration of interactive aerosols into operational weather
614 prediction models, a relatively new development, may help stimulate progress in this
615 area.

616

617 In answer to the last question raised in the introduction, the VOCA comparison presented
618 here demonstrates that VOCALS-REx observations provide a good benchmark for
619 aerosols and for cloud properties, providing a comprehensive observational basis for a
620 first order look at aerosol-cloud interactions in a broad range of models. Future

621 comparisons using VOCALS-REx data or other field data could aim at better quantitative
622 constraints on individual aerosol and cloud processes by enforcing more uniform land
623 and ocean surface emission conditions and possibly specifying lateral advective
624 conditions. Because of the large numbers of model fields and high resolution outputs of
625 some models, the overall utility of the intercomparison could be improved by adding an
626 additional quality-assurance phase to the submission process, where model setup and
627 output over a relatively short simulation period could be evaluated and corrected prior to
628 conducting experiments over long durations. Collection of additional model outputs, such
629 as a broader selection of CCN activation supersaturations, more detailed aerosol size
630 information, and rates of aerosol-related processes could be used to help better unravel
631 individual model biases. An alternative but promising approach for some categories of
632 models would be a variation of a kinematic driver framework (KiD, Shipway and Hill
633 2012) in order to analyze and compare microphysical and aerosol processes in various
634 models.

635

636

637

638 **Appendix: Model Descriptions**

639

640 NCAR CAM4 and CAM5 are both part of the CESM1.0 release. The global NCAR
641 CAM4 and CAM5 simulations were performed with similar setups with the finite volume
642 dynamical core. Both use daily forecast runs initialized with ECMWF YOTC analyses
643 interpolated onto the model grid, and are analyzed at hours 48-72. They use identical

644 horizontal resolution, but with fewer vertical levels in CAM4, especially in the boundary
645 layer. CAM4 uses a prognostic (liquid and ice) single moment microphysics scheme
646 (Rasch and Kristjansson, 1998). CAM5 uses the two-moment prognostic bulk scheme
647 including prognostic number concentration (Gettelman et al. 2008; Morrison and
648 Gettelman, 2008). The PBL schemes also differ: CAM4 uses the non-local diffusivity
649 scheme (Holtslag and Boville, 1993) while CAM5 uses the TKE based turbulence
650 scheme of Bretherton and Park (2009) and the shallow convection scheme of Park and
651 Bretherton (2009).

652

653 CAM4 is run here with a bulk aerosol scheme (MOZART, Lamarque et al. 2005 while
654 CAM5 uses a prognostic aerosol model with three modes (MAM3). For sea-salt, CAM4
655 uses 4 bins, with sea-surface emission following Mahowald et al. (2006). CAM5 uses the
656 sea-salt emission parameterization of Martensson et al. (2003). For SO₂ emissions CAM4
657 uses Smith et al. (2001) while CAM5 uses Smith et al. (2004). For carbon emissions
658 CAM4 uses Liousse et al. (1996) and Cooke et al. (1999), while CAM5 follows Bond et
659 al. (2007) and Junker and Liousse (2008). For other land anthropogenic emissions,
660 CAM5 uses the IPCC AR5 emissions (Lamarque et al. 2010). CAM4 uses a very similar
661 radiation scheme to CAM 3 (Collins et al. 2006), while CAM5 uses the RRTMG scheme
662 (Iacono et al. 2008) with a McICA approach. More detailed descriptions of CAM4 and
663 CAM5 radiation, MAM3 and other physics can be found at

664 <http://www.cesm.ucar.edu/models/>.

665

666 The IPRC model iRAM 1.2 is very similar to the version described in Lauer et al. (2009)
667 but run at higher horizontal resolution ($0.25^{\circ} \times 0.25^{\circ}$). The simulations here used NCEP
668 Final Analysis (FNL) for initial and boundary conditions. Monthly mean aerosol
669 concentrations are prescribed for these simulations based on global model simulations of
670 aerosol mass (see Lauer et al. 2007) and observed aerosol size distributions (see
671 McNaughton 2008). Cloud microphysics are calculated with a two-moment bulk scheme
672 (Phillips et al. 2007, 2008, 2009). Aerosol activation is tracked and affects cloud
673 microphysics, but cloud evolution and precipitation do not affect aerosol mass
674 concentrations or sizes outside of clouds. The PBL scheme uses a turbulence closure with
675 prognostic turbulent kinetic energy (TKE) and dissipation rate (Detering and Etling 1985;
676 Langland and Liou 1996). The radiation scheme is based on Edwards and Slingo (1996).
677
678 The three WRF Chem simulations were run continuously over the study period and have
679 similarly sized domains. UW and IOWA use NCEP FNL analyses and PNNL uses NCEP
680 GFS analyses for initial and boundary conditions together with MOZART model output
681 for initializing concentrations of chemical species and aerosols. All use the VOCA
682 standard anthropogenic and volcanic land emissions. All use the RRTM scheme (Mlawer
683 et al., 1997) for LW radiation and the Goddard scheme (see Chou et al. 1998) for SW
684 radiation. However the three simulations' horizontal and vertical resolutions differ, as do
685 many of their other aerosol, cloud, and boundary layer physics parameterizations.
686
687 The IOWA run uses WRF Chem v3.3, and its configuration and physics are described in
688 detail in Saide et al. (2012). The MOSAIC (Zaveri et al. 2008) 8-bin sectional aerosol

689 scheme is used, with the CBM-Z gas-phase chemical mechanism (Zaveri and Peters,
690 1999) and modified DMS reactions. Biogenic land emissions are based on the MEGAN
691 algorithm (Guenther et al., 2006) and biomass burning emissions are estimated from
692 FIRMS MODIS fire detections (Davies et al., 2009). A bulk two-moment Lin
693 microphysics scheme (see Chapman et al. 2009) and a level-2.5 Mellor-Yamada-type
694 PBL scheme (MYNN 2.5, Nakanishi and Niino 2004) are used.

695

696 The PNNL simulation uses modified WRF Chem v3.2.1 code, which was later released to
697 the public in v3.3. The model is configured to use the MOSAIC 8-bin sectional aerosol
698 module and the CBM-Z mechanism with DMS chemistry. The PNNL runs also use
699 biogenic and biomass burning emissions from MEGAN and MODIS, respectively. The
700 PNNL simulations differ in the use of the bulk two-moment microphysics scheme of
701 Morrison (Morrison and Gettelman, 2008) and the YSU non-local PBL scheme (Hong et
702 al., 2006). Additional details regarding the model's physical parameterizations and
703 configuration for the PNNL simulations can be found in Q. Yang et al. (2011 and 2012).

704

705 The UW contribution also uses WRF Chem v3.2.1, though on a coarser horizontal and
706 vertical grid than the IOWA and PNNL runs. Aerosols are represented with 3 modes
707 using the Modal Aerosol Dynamics Model for Europe (MADE, Ackerman et al., 1998)
708 together with a Secondary Organic Aerosol Model (SORGAM, Schell et al. 2001). The
709 Regional Acid Deposition Model, version 2 (RADM2) (Chang et al., 1989) chemical
710 mechanism is used with modified DMS reactions. The UW run neglects biogenic and
711 biomass burning emissions. For DMS flux, the UW run follows the VOCA specification.

712 The same Lin microphysics scheme is used as the IOWA runs. Like CAM5, the TKE
713 scheme of Bretherton and Park (2009) is used in the PBL but no shallow convection
714 scheme is used.

715

716 The UKMO simulations use a deterministic global numerical weather prediction (NWP)
717 configuration of the Met Office Unified Model (MetUM) (Davies et al., 2005) based on
718 that in the Met Office's operational NWP suite between 9th March and 14th July 2010;
719 this is designated global NWP cycle G52. Two main forecasts were run per day, each 5
720 days in length, initialized at 00UTC and 12UTC, for which the first 12 hours are analyzed
721 in this study. The Coupled Large-scale Aerosol Simulator for Studies in Climate
722 (CLASSIC) prognostic aerosol scheme from the Met Office Hadley Centre was used
723 (Bellouin et al. 2011). Aerosol concentrations are initialized from HadGEM-2
724 climatologies from a 20-year HadGEM2 climate run with the CLASSIC scheme. Aerosol
725 emissions used are based on the AeroCom-2 hindcast emissions (Diehl et al., 2012) based
726 on the year 2006. DMS emissions come from HadGEM2-based climatology. Local SSA
727 over the ocean are diagnosed based on surface wind speed, and are not transported or
728 deposited. Biogenic land aerosol is not modeled explicitly but instead comes from a
729 climatology based on earlier simulations. A single moment bulk microphysics scheme
730 (Wilson and Ballard, 1999), the Lock et al. PBL (2000) scheme, and the 2-stream
731 radiation scheme of Edwards and Slingo (1996) were used.

732

733 The ECMWF runs use the Monitoring Atmospheric Composition and Climate (MACC)
734 cycle model 36R1. Full model documentation is available at

735 <http://www.ecmwf.int/research/ifsdocs/CY33r1/index.html>. Daily 24-hour forecast runs
736 are used with aerosols in the model as passive tracers. The model uses the aerosol scheme
737 of Morcrette et al. (2009), which has 3 bins each for sea-salt and dust, single prognostic
738 variables for SO₂ and SO₄, and 12 prognostic variables in all. The ECMWF model uses a
739 bulk single-moment microphysics scheme. The RRTM radiation scheme is used with a
740 McICA approach (Morcrette et al. 2008). The PBL in the model uses an eddy-diffusivity
741 mass-flux framework (Köhler et al. 2011).

742

743 The GFDL AM3 (Donner et al. 2011) was run in forecast mode on a cubed-sphere
744 48x48x6 grid with model output originally interpolated to a 2.0° latitude x 2.5° longitude
745 grid. The runs were initialized with ECMWF reanalysis data. The GFDL modal aerosol
746 scheme uses two modes for sulfate and organic aerosol, and three modes for sea salt (see
747 Donner et al. 2011). Anthropogenic emissions are estimated from historical values of
748 Lamarque et al. (2010). Biogenic emissions and DMS emissions from the ocean surface
749 are also included. The microphysics scheme follows Rotstayn (1997) and Rotstayn et al.
750 (2000) including prognostic cloud number concentration (Ming et al. 2006). The Lock et
751 al. (2000) PBL scheme is used. The radiation scheme used is due to Freidenreich and
752 Ramaswamy (1999) and Schwarzkopf and Ramaswamy (1999). See Donner et al. (2011)
753 for more details.

754

755

756

757

758 **Acknowledgements**

759

760 The authors wish to thank Grant Allen for his providing of aircraft data for many of the
761 figures. Thanks also to Romain Blot for providing sea salt measurements. Thanks to Matt
762 Lebsack for providing CloudSat precipitation data and Dan Grosvenor for his assistance.
763 The comments of two anonymous reviewers helped improve this paper. The portion of
764 this work conducted at University of Iowa was carried out with the aid of NASA grants
765 NNX08AL05G and NNX11AI52G, EPA grant 83503701, grant number UL1RR024979
766 from the National Center for Research Resources (NCRR), a part of the National
767 Institutes of Health (NIH), and Fulbright-CONICYT scholarship number 15093810. Its
768 contents are solely the responsibility of the authors and do not necessarily represent the
769 official views of the founding institutions. Funding for Pacific Northwest National
770 Laboratory (PNNL) contributions to this research has been provided by the US National
771 Oceanic and Atmospheric Administration (NOAA) Atmospheric Composition and
772 Climate Program (NA10AANRG0083/56091). PNNL is operated for DOE by Battelle
773 Memorial Institute under Contract No. DE-AC05-76RL01830.

774

References

- Abdul-Razzak, H., and Ghan, S. J.: A parameterization of aerosol activation. 3. Sectional representation, *J. Geophys. Res.*, 107, D3, AAC 1-1-AAC 1-6, 2002.
- Abel, S. J., Walters, D. N., and Allen, G.: Evaluation of stratocumulus cloud prediction in the Met Office forecast model during VOCALS-Rex, *Atmos. Chem. Phys.*, 10, 10541-10559. doi:10.5194/acp-10-10541-2010, 2010.
- Ackermann, I. J., Hass, H., Memmesheimer, M., Ebel, A., Binkowski, F. S., and Shankar, U.: Modal aerosol dynamics model for Europe: development and first applications, *Atmos. Env.*, 32, 2981-2999, doi:10.1016/S1352-2310(98)00006-5, 1998.
- Allen, G. and co-authors, 2011: South East Pacific atmospheric composition and variability sampled along 20S during VOCALS-Rex, *Atmos. Chem. Phys.*, 11, 5237-5262.
- Bellouin, N., Boucher, O., Haywood, J., Johnson, C., Jones, A., Rae, J., and Woodward, S.: Improved representation of aerosols for HadGEM2, Tech. Note 73, Hadley Cent. Met Office, Exeter, UK., 2007.
- Bellouin, N., Rae, J., Jones, A., Johnson, C., Haywood, J., and Boucher, O.: Aerosol forcing in the Climate Model Intercomparison Project CMIP5 simulations by HadGEM2-ES and the role of ammonium nitrate, *J. Geophys. Res.*, 116, D20 206, doi:10.1029/2011JD016074, 2011.
- Blot, R., Clarke, A. D., Freitag, S., Kapustin, V., Howell, S. G., Jensen, J. B., Shank, L. M., McNaughton, C. S., and Brekhovskikh, V.: Ultrafine sea spray aerosol over the south eastern Pacific: open-ocean contributions to marine boundary layer CCN, *Atmos. Chem. Phys.*, 13, 7263-7278, doi:10.5194/acp-13-7263-2013, 2013.
- Bond, T. C., Bhardwaj, E., Dong, R., Jogani, R., Jung, S., Roden, C., Streets, D. G., and Trautmann, N. M.: Historical emissions of black and organic carbon aerosol from energy-related combustion, 1850–2000, *Global Biogeochem. Cycles*, 21, GB2018, doi:10.1029/2006GB002840, 2007.
- Boyle, J., Klein, S., Zhang, G., Xie, S., and Wei, X.: Climate model forecast experiments for TOGA COARE. *Mon. Wea. Rev.*, 136, 808–832. doi: <http://dx.doi.org/10.1175/2007MWR2145.1>, 2008.
- Bretherton, C. S. and Park, S.: A new moist turbulence parameterization in the Community Atmosphere Model, *J. Climate*, 22, 3422-3448, 2009.
- Bretherton, C. S., T. Uttal, C. W. Fairall, S. Yuter, R. Weller, D. Baumgardner, K. Comstock, R. Wood, and Raga, G.: The EPIC 2001 stratocumulus study. *Bull. Amer. Meteor. Soc.*, 85, 967-977, 2004.

Bretherton, C. S., Wood, R., George, R. C., Leon, D., Allen, G., and Zheng, X.: Southeast Pacific stratocumulus clouds, precipitation, and boundary layer structure sampled along 20° S during VOCALS-Rex. *Atmos. Chem. Phys.*, 10, 10639-10654. doi:10.5194/acp-10-10639-2010, 2010.

Burleyson, C. D., de Szoeko, S. P., Yuter, S. E., Wilbanks, M., and Brewer, W. A.: Ship-based observations of the diurnal cycle of southeast Pacific marine stratocumulus clouds and precipitation, *J. Atmos. Sci.*, 70, 3876-3894, doi:10.1175/JAS-D-13-01.1, 2013.

Chang, J. S., Binkowski, F. S., Seaman, N. L., McHenry, J. N., Samson, P. J., Stockwell, W. R., Walcek, C. J., Madronich, S., Middleton, P. B., Pleim, J. E., and Lansford, H. H.: The regional acid deposition model and engineering model. State-of-Science/Technology, Report 4, National Acid Precipitation Assessment Program, Washington D.C., 1989.

Chapman, E. G., Gustafson Jr., W. I., Easter R. C., Barnard, J. C., Ghan, S. J., Pekour, M. S., Fast, J. D.: Coupling aerosol-cloud-radiative processes in the WRF-chem model: Investigating the radiative impact of large point sources, *Atmos. Chem. Phys.*, 9, 945-964, 2009.

Chou, M. D., Suarez, M. J., Ho, C. H., Yan, M. M. H., and Lee, K. T.: Parameterizations for cloud overlapping and shortwave single-scattering properties for use in general circulation and cloud ensemble models, *J. Climate*, 11, 202–214, 1998.

Clarke, A. D., Owens, S. R., and Zhou, J.: An ultrafine sea-salt flux from breaking waves: Implications for cloud condensation nuclei in the remote marine atmosphere., *J. Geophys. Res.*, 111, doi:10.1029/2005JD006565, 2006.

Clarke, A. D., Freitag, S., Brekhovskikh, V., Campos, T., Snider, J. R., Kasputin, V., Howell, S., Shank, L., and McNaughton, C.: Combustion aerosol, entrainment, and clouds in the VOCALS region, *CLIVAR Exchanges*, 15, 25-28, 2010.

Collins, W. D., Bitz, C. M., Blackmon, M. L., Bonan, G. B., Bretherton, C. S., Carton, J. A., Chang, P., Doney, S. C., Hack, J. J., Henderson, T. B., Kiehl, J. T., Large, W. G., McKenna, D. S., Santer, B. D., and Smith, R. D.: The community climate system model version 3 (CCSM3), *J. Climate*, 19, 2122-2143, 2006.

Cooke, W. F., Liousse, C., and Cachier, H.: Construction of a 1° x 1° fossil fuel emission data set for carbonaceous aerosol and implementation and radiative impact in the ECHAM4 model, *J. Geophys. Res.*, 104(D18), 22137-22162, doi:10.1029/1999JD900187, 1999.

Davies, T., Cullen, M. J. P., Malcolm, A. J., Mawson, M. H., Staniforth, A., White, A. A., and Wood, N.: A new dynamical core for the Met Office's global and regional modeling of the atmosphere, *Q. J. R. Met. Soc.*, 131, 1759-1782, 2005.

Davies, D. K., Ilavajahala, S., Wong, M. M., and Justice, C. O.: Fire Information for Resource Management System: Archiving and distributing MODIS active fire data, *IEEE Trans. Geosci. Remote Sens.*, 47, 72-79, doi:10.1109/TGRS.2008.2002076, 2009.

Detering, H. W., and Etling, D.: Application of the E- ϵ turbulence model to the atmospheric boundary layer, *Bound.-Layer Meteor.*, 33, 113-133, 1985.

de Szoeke, S. P., Yuter, S., Mechem, D., Fairall, C. W., Burleyson, C. D., and Zuidema, P.: Observations of stratocumulus clouds and their effect on the eastern pacific surface heat budget along 20°S, *J. Climate*, 25, 8542-8567, doi: 10.1175/JCLI-D-11-00618.1, 2012.

Diehl, T., Heil, A., Chin, M., Pan, X., Streets, D., Schultz, M., and Kinne, S.: Anthropogenic, biomass burning, and volcanic emissions of black carbon, organic carbon, and SO₂ from 1980 to 2010 for hindcast model experiments, *Atmos. Chem. Phys. Discuss.*, 12, 24 895–24 954, doi:10.5194/acpd-12-24895-2012, 2012.

Donner, L. J., Wyman, B. L., Hemler, R. S. and 38 co-authors, 2011: The dynamical core, physical parameterizations, and basic simulation characteristics of the atmospheric component AM3 of the GFDL Global Coupled Model CM3. *J. Climate.*, 24, 3484-3519, 2011.

Edwards, J. M., and Slingo, A., Studies with a flexible new radiation code. I: Choosing a configuration for a large-scale model, *Quart. J. Roy. Meteor. Soc.*, 122, 689-719, 1996.

Emmons, L. K., Walters, S., Hess, P. G., Lamarque, J.-F., Pfister, G. G., Fillmore, D., Granier, C., Guenther, A., Kinnison, D., Laepple, T., Orlando, J., Tie., X., Tyndall, G., Wiedinmyer, C., Baughcum, S. L., and Kloster, S.: Description and evaluation of the Model for Ozone and Related chemical Tracers, version 4 (MOZART-4), *Geosci. Model Dev.*, 3, 43-67, doi:10.5194/gmd-3-43-2010, 2010.

Freidenreich, S. M., and Ramaswamy, V.: A new multiple-band solar radiative parameterization for general circulation models, *J. Geophys. Res.*, 104, 31389-31409, 1999.

George, R. C., and Wood, R.: Subseasonal variability of low cloud radiative properties over the southeast Pacific Ocean, *Atmos. Chem. Phys.*, 10, 4047-4063, doi:10.5194/acp-10-4047-2010, 2010.

George, R. C., Wood, R., Bretherton, C. S., and Painter, G.: Development and impact of hooks of large droplet concentration on remote southeast Pacific stratocumulus, *Atmos. Chem. Phys.*, 13, 6305-6328, doi:10.5194/acp-13-6305-2013, 2013.

Gettelman, A., Morrison, H., and Ghan, S. J.: A new two-moment bulk stratiform cloud microphysics scheme in the Community Atmospheric Model, Version 3 (CAM3). Part II: Single-column and global results, *J. Climate*, 21, 3660-3679, 2008.

Gong, S. L., Barrie, L. A., and Blanchet, J.-P.: Modeling sea-salt aerosols in the atmosphere. 1. Model development. *J. Geophys. Res.*, 102, D3, 3805-3818, 1997.

Guenther, A., Karl, T., Harley, P., Wiedinmyer, C., Palmer, P. I., and Geron, C.: Estimates of global terrestrial isoprene emissions using MEGAN (Model of Emissions of Gases and Aerosols from Nature), *Atmos. Chem. Phys.*, 6, 3181-3210, doi:10.5194/acp-6-3181-2006, 2006.

Hannay, C., Williamson, D. L., Hack, J. J., Kiehl, J. T., Olson, J. G., Klein, S. A., Bretherton, C. S., and Köhler, M.: Evaluation of forecasted Southeast Pacific stratocumulus in the NCAR, GFDL, and ECMWF models. *J. Climate*, 22, 2871–2889. doi: <http://dx.doi.org/10.1175/2008JCLI2479.1>, 2009.

Holtstlag, A. A. M. and Boville, B. A.: Local versus nonlocal boundary-layer diffusion in a global climate model, *J. Climate*, 6, 1825-1842, 1993.

Hong, S.-Y., Noh, Y., and Dudhia, J.: A new vertical diffusion package with an explicit treatment of entrainment processes, *Mon. Wea. Rev.*, 134, 2318-2341, 2006.

Hudson, J. G., Noble, S., and Jha, V.: Stratus cloud supersaturations, *Geophys. Res. Lett.*, 37, L21813, doi:10.1029/2010GL045197, 2010.

Iacono, M. J., Delamere, J. S., Mlawer, E. J., Shephard, M. W., Clough, S. A., and Collins, W. D.: Radiative forcing by long-lived greenhouse gases: Calculations with the AER radiative transfer models, *J. Geophys. Res.*, 113, D13103, doi:10.1029/2008JD009944, 2008.

Junker, C., and Liou, S. C.: A global emission inventory of carbonaceous aerosol from historic records of fossil fuel and biofuel consumption for the period 1860–1997, *Atmos. Chem. Phys.*, 8, 1195-1207, doi:10.5194/acp-8-1195-2008, 2008.

Köhler, M., Ahlgrimm, M., and Beljaars, A.: Unified treatment of dry convective and stratocumulus-topped boundary layers in the ECMWF model, *Quart. J. Roy. Meteor. Soc.*, 137, 43-57, doi:10.1002/qj.713, 2011.

Lauer, A., Eyring, V., Hendricks, J., Jöckel, P., and Lohmann, U.: Global model simulations of the impact of ocean-going ships on aerosols, clouds, and the radiation budget, *Atmos. Chem. Phys.*, 7, 1-19, 2007.

Lauer, A., Wang, Y., Phillips, V. T. J., McNaughton, C. S., Bennartz, R., and Clarke, A. D.: Simulating marine boundary layer clouds over the eastern Pacific in a regional

climate model with double-moment cloud microphysics, *J. Geophys. Res.*, 114, D21205, doi:10.1029/2009JD012201, 2009.

Lamarque, J.-F., Kiehl, J. T., Brasseur, G. P., Butler, T., Cameron-Smith, P., Collins, W. D., Collins, W. J., Granier, C., Hauglustaine, D., Hess, P. G., Holland, E. A., Horowitz, L., Lawrence, M. G., McKenna, D., Merilees, P., Prather, M. J., Rasch, P. J., Rotman, D., Shindell, D., and Thornton, P.: Assessing future nitrogen deposition and carbon cycle feedback using a multimodel approach: analysis of nitrogen deposition, *J. Geophys. Res.*, 110, D19303, doi: 10.1029/2005JD005825, 2005.

Lamarque, J.-F., and 21 co-authors: Historical (1850-2000) gridded anthropogenic and biomass burning emissions of reactive gasses and aerosols: methodology and application, *Atmos. Chem. Phys.*, 10, 7017-7039. doi:10.5194/acp-10-7017-2010, 2010.

Langland, R. H., and Liou, C.-S.: Implementation of an E- ϵ parameterization of vertical subgrid-scale mixing in a regional model, *Mon. Wea. Rev.*, 124, 905-918, 1996.

Liousse, C., Penner, J. E., Chuang, C., Walton, J. J., Eddleman, H., and Cachier, H.: A global three-dimensional model study of carbonaceous aerosols, *J. Geophys. Res.*, 101(D14), 19411–19432, doi:10.1029/95JD03426, 1996.

Lock, A. P., Brown, A. R., Bush, M. R., Martin, G. M., and Smith, R. N. B.: A new boundary layer mixing scheme. Part I: scheme description and single-column model tests, *Mon. Wea. Rev.*, 128, 3187-3199, 2000.

Mahowald, N. M., Lamarque, J.-F., Tie, X.X., Wolff, E.: Sea-salt aerosol response to climate change: Last Glacial Maximum, preindustrial, and doubled carbon dioxide climates, *J. Geophys. Res.*, 111, D05303, doi: 10.1029/2005JD006459, 2006.

Mårtensson, E. M., Nilsson, E. D., de Leeuw, G., Cohen, L. H., and Hansson, H. C.: Laboratory simulations and parameterization of the primary marine aerosol production, *J. Geophys. Res.*, 108, 4297, doi: 10.1029/2002JD002263, 2003.

Martin, G. M., Johnson, D. W., and Spice, A.: The measurement and parameterization of effective radius of droplets in warm stratocumulus clouds. *J. Atmos. Sci.*, 51, 1823–1842, 1994.

McNaughton, C. S.: Constraining climate model simulations of aerosol size distributions over the North Pacific and North America using in-situ airborne measurements, Ph. D. thesis, Univ. of Hawaii at Manoa, Honolulu, Hawaii, USA, 2008.

Mechoso, C. R., Wood, R., Weller, R., Bretherton, C. S., Clarke, A. D., Coe, H., Fairall, C., Farrar, J. T., Feingold, G., Garreaud, R., Grados, C., McWilliams, J., de Szoeke, S. P., Yuter, S. E., Zuidema, P.: Ocean-cloud-atmosphere-land interactions in the southeastern Pacific: The VOCALS Program. *Bull. Amer. Meteor. Soc.*, 95, 357-375, doi: 10.1175/BAMS-D-11-00246.1, 2014.

Mena-Carrasco, M., Oliva, E., Saide, P., Spak, S. N., de la Maza, C., Osses, M., Tolvett, S., Campbell, J. E., Tsao, T. C.-C., and Molina, L. T.: Estimating the health benefits from natural gas use in transport and heating in Santiago, Chile, *Sci. Tot. Env.*, 429, 257-265, doi: 10.1016/j.scitotenv.2012.04.037, 2012.

Ming, Y., V. Ramaswamy, V., Donner, L. J., and Phillips, V. T. J.: A new parameterization of cloud droplet activation applicable to general circulation models. *J. Atmos. Sci.*, 63, 1348-1356, 2006.

Mlawer, E.J., Taubman, S.J., Brown, P.D., Iacono, M.J., and Clough, S.A.: Radiative transfer for inhomogeneous atmosphere: RRTM, a validated correlated-k model for the longwave. *J. Geophys. Res.*, 102, 16663-16682, 1997.

Monahan, E. C., Spiel, D. E., and Davidson, K. L.: A model of marine aerosol generation via whitecaps and wave disruption, in *Oceanic Whitecaps and Their Role in Air-Sea Exchange Processes*, edited by E. C. Monahan and G. Mac Niocaill, pp. 167-193, Springer, New York, 1986.

Morcrette, J.-J., Barker, H. W., Cole, J. N. S., Iacono, M. J., and Pincus, R.: Impact of a new radiation package, McRad, in the ECMWF Integrated Forecasting System. *Mon. Wea. Rev.*, 136, 4773-4798, doi: 10.1175 /2008MWR2363.1, 2008.

Morcrette, J.-J., Boucher, O., Jones, L., Salmond, D., Bechtold, P., Beljaars, A., Benedetti, A., Bonet, A., Kaiser, J. W., Razinger, M., Schulz, M., Serrar, S., Simmons, A. J., Sofiev, M., Suttie, M., Tompkins, A.M., Untch, A.: Aerosol analysis and forecast in the ECMWF Integrated Forecast System: Forward modelling. *J. Geophys. Res.*, 114, D06206, doi: 10.1029 /2008JD011235, 2009.

Morrison, H., and Gettelman, A.: A new two-moment bulk stratiform cloud microphysics scheme in the Community Atmosphere Model, version 3 (CAM3). Part I: description and numerical tests, *J. Climate*, 21, 3642-3659, 2008.

Nakanishi, M. and Niino, H.: An improved Mellor-Yamada level-3 model with condensation physics: its design and verification. *Bound. Layer Meteor.*, 112, 1-31, 2004.

Nightingale, P. D., Malin, G., Law, C. S., Watson, A. J., Liss, P. S., Liddicoat, M. I., Boutin, J., and Upstill-Goddard, R. C.: In situ evaluation of air-sea gas exchange parameterizations using novel conservative and volatile tracers. *Glob. Biogeochem. Cyc.*, 14, 373-387, 2000.

Ovchinnikov, M., Easter, R. C., and Gustafson, W. I.: Untangling dynamical and microphysical controls for the structure of stratocumulus. *Geophys. Res. Lett.*, 40, 4432-4436, doi:10.1002/grl.50810, 2013.

Park, S. and Bretherton, C. S.: The University of Washington shallow convection and moist turbulence schemes and their impact on climate simulations with the community atmosphere model, *J. Climate*, 22, 3449-3469, 2009.

Phillips, T. J., Potter, G. L., Williamson, D. L., Cederwall, R. T., Boyle, J. S., Fiorino, M., Hnilo, J. J., Olson, J. G., Xie, S., and Yio, J. J.: Evaluating parameterizations in general circulation models: climate simulation meets weather prediction. *Bull. Amer. Meteor. Soc.*, 85, 1903–1915. doi: <http://dx.doi.org/10.1175/BAMS-85-12-1903>, 2004.

Phillips, V. T. J., Donner, L. J., and Garner, S. T.: Nucleation processes in deep convection simulated by a cloud-system-resolving model with double-moment bulk microphysics, *J. Atmos. Sci.*, 64, 738-761, doi:10.1175/JAS3869.1, 2007.

Phillips, V. T. J., DeMott, P. J., and Andronache, C.: An empirical parameterization of heterogeneous ice nucleation for multiple chemical species of aerosol, *J. Atmos. Sci.*, 65, 2757-2783, doi:10.1175/2007JAAS2546.1, 2008.

Phillips, V. T. J., Andronache, C., Christner, B., Morris, C. E., Sands, D. C., Bansemer, A., Lauer, A., McNaughton, C., and Seman, C.: Potential impacts from biological aerosols on ensembles of continental clouds simulated numerically, *Biogeosciences*, 6, 987-1014, 2009.

Rapp, A. D., Lebsock, M., and L'Ecuyer, T.: Low cloud precipitation climatology in the southeastern Pacific marine stratocumulus region using CloudSat, *Environ. Res. Lett.*, 8, 014027, doi:10.1088/1748-9326/8/1/014027, 2013.

Rasch, P. J. and Kristjánsson, J. E.: A comparison of the CCM3 model climate using diagnosed and predicted condensate parameterizations, *J. Climate*, 11, 1587-1614, 1998.

Richter, I. and Mechoso, C. R.: Orographic influences on subtropical stratocumulus, *J. Atmos. Sci.*, 63, 2585–2601, 2006.

Rotstayn, L. D.: A physically based scheme for the treatment of stratiform clouds and precipitation in large-scale models. I: Description and evaluation of the microphysical processes, *Q. J. Roy. Met. Soc.*, 123, 1227-1282, 1997.

Rotstayn, L. D.: On the “tuning” of autoconversion parameterizations in climate models, *J. Geophys. Res.*, 105, 15495-15507, 2000.

Saide, P. E., Spak, S. N., Carmichael, G. R., Mena-Carrasco, M. A, Yang, Q., Howell, S., Leon, D. C., Snider, J. R., Bandy, A. R., Collett, J. L., Benedict, K. B., de Szoeko, S. P., Hawkins, L. N., Allen, G., Crawford, I., Crosier, J., and Springston, S. R.: Evaluating WRF-Chem aerosol indirect effects in Southeast Pacific marine stratocumulus during VOCALS-Rex. *Atmos. Chem. Phys.*, 12, 3045-3064. doi:10.5194/acp-12-3045-2012, 2012.

- Schell B., Ackermann, I. J., Hass, H., Binkowski, F. S., and Ebel, A.: Modeling the formation of secondary organic aerosol within a comprehensive air quality model system, *J. Geophys. Res.*, 106, 28275-28293, 2001.
- Schwarzkopf, M. D., and Ramaswamy, V.: Radiative effects of CH₄, N₂O, halocarbons, and the foreign-broadened H₂O continuum: A GCM experiment, *J. Geophys., Res.*, 104, 9467-9488, 1999.
- Shank, L. M., Howell, S., Clarke, A. D., Freitag, S., Brekhovskikh, V., Kapustin, V., McNaughton, C., Campos, T., and Wood, R.: Organic matter and non-refractory aerosol over the remote Southeast Pacific: oceanic and combustion sources, *Atmos. Chem. Phys.*, 12, 557-576, doi:10.5194/acp-12-557-2012, 2012.
- Shipway, B. J., and Hill, A. A.: Diagnosis of systematic differences between multiple parametrizations of warm rain microphysics using a kinematic framework, *Q. J. R. Meteorol. Soc.*, 138, 2196-2211, 2012.
- Smith, S. J., Pitcher, H., and Wigley, T. M. L.: Global and regional anthropogenic sulfur dioxide emissions, *Glob. Biogeochem. Cy.*, 29, 99-119, 2001.
- Smith, S. J., Andres, R., Conception, E., and Lurz, J.: Historical sulfur dioxide emissions 1850-2000: methods and results, Technical report, Pacific Northwest National Laboratory, Joint Global Change Research Institute, College Park, MD, USA, 2004.
- Snider, J. R., Guibert S., Brenguier, J.-L., and Putaud, J.-P.: Aerosol activation in marine stratocumulus clouds: 2. Köhler and parcel theory closure studies, *J. Geophys. Res.*, 108(D15), 8629, doi:10.1029/2002JD002692, 2003.
- Twohy, C. H., Anderson, J. R., Toohey, D. W., Andrejczuk, M., Adams, A., Lytle, M., George, R. C., Wood, R., Saide, P., Spak, S., Zuidema, P., and Leon, D.: Impacts of aerosol particles on the microphysical and radiative properties of stratocumulus clouds over the southeast Pacific Ocean. *Atmos. Chem. Phys.*, 13, 2541-2562, doi:10.5194/acp-13-2541-2013, 2013.
- Wang, S., O'Neill, L. W., Jiang, Q., de Szoeko, S. P., Hong, X., Jin, H., Thompson, W. T., and Zheng, X.: A regional real-time forecast of marine boundary layers during VOCALS-REx, *Atmos. Chem. Phys.*, 11, 421-437, doi:10.5194/acp-11-421-2011, 2011.
- Wilson, D. R. and Ballard, S. P.: A microphysically based precipitation scheme for the UK Meteorological Office Unified Model, *Q. J. Roy. Met. Soc.*, 125, 1607-1636, 1999.
- Wood, R., Comstock, K. K., Bretherton, C. S., Cornish, C., Tomlinson, J., Collins D. R., and Fairall, C.: Open cellular structure in marine stratocumulus cloud sheets. *J. Geophys. Res.*, **113**, D12207, doi:10.1029/2007JD009371, 2008

- Wood, R. and 33 co-authors: The VAMOS Ocean-Cloud-Atmosphere-Land Study Regional Experiment (VOCALS-REx): goals, platforms, and field operations. *Atmos. Chem. Phys.*, 11, 627-654. doi:10.5194/acp-11-627-2011, 2011a.
- Wood, R., Bretherton, C. S., Leon, D., Clarke, A. D., Zuideman, P., Allen, G., and Coe, H.: An aircraft case study of the spatial transition from closed to open mesoscale cellular convection over the Southeast Pacific. *Atmos. Chem. Phys.*, 11, 2341-2370. doi: 10.5194/acp-11-2341-2011, 2011b.
- Wood, R., Leon, D., Lebsock, M., Snider, J., and Clarke, A. D.: Precipitation driving of droplet concentration variability in marine low clouds, *J. Geophys. Res.*, 117, D19210, doi:10.1029/2012JD018305, 2012.
- Wyant, M. C. and 20 co-authors, 2010: The PreVOCA experiment: modeling the lower troposphere in the Southeast Pacific, *Atmos. Chem. Phys.*, 10, 4757-4774, doi:10.5194/acp-10-4757-2010
- Yang, M., Huebert, B. J., Blomquist, B. W., Howell, S. G., Shank, L. M., McNaughton, C. S., Clarke, A. D., Hawkins, L. N., Russell, L. M., Covert, D. S., Coffman, D. J., Bates, T. S., Quinn, P. K., Zagorac, N., Bandy, A. R., de Szoeko, S. P., Zuideman, P. D., Tucker, S. C., Brewer, W. A., Benedict, K. B., and Collett, J. L.: Atmospheric sulfur cycling in the southeastern Pacific – longitudinal distribution, vertical profile, and diel variability observed during VOCALS-REx, *Atmos. Chem. Phys.*, 11, 5079-5097, doi:10.5194/acp-11-5079-2011, 2011.
- Yang, Q., Gustafson Jr., W. I., Fast, J. D., Wang, H., Easter, R. C., Morrison, H., Lee, Y.-N., Chapman, E. G., Spak, S. N., and Mena-Carrasco, M. A.: Assessing regional scale predictions of aerosols, marine stratocumulus, and their interactions during VOCALS-Rex using WRF-Chem. *Atmos. Chem. Phys.*, 11, 11951-11975, doi: 10.5194/acp-11-11951-2011, 2011.
- Yang, Q., Gustafson Jr., W. I., Fast, J. D., Wang, H., Easter, R. C., Wang, M., Ghan, S. J., Berg, L. K., Leung, L. R., and Morrison, H.: Impact of natural and anthropogenic aerosols on stratocumulus and precipitation in the Southeast Pacific: a regional modelling study using WRF-Chem, *Atmos. Chem. Phys.*, 12, 8777-8796, doi:10.5194/acp-12-8777-2012, 2012.
- Zaveri, R. A., and Peters, L. K.: A new lumped structure photochemical mechanism for large-scale applications, *J. Geophys. Res.*, 104, 30387 – 30415, 1999.
- Zaveri, R. A., Easter, R. C., Fast, J. D., Peters, L.: Model for simulating aerosol interactions and chemistry (MOSAIC), *J. Geophys. Res.*, 113, D13204, doi: 10.1029/2007JD008782, 2008
- Zuidema, P., Leon, D., Pazmany, A., and Cadetdu, M.: Aircraft millimeter-wave passive sensing of cloud liquid water and water vapor during VOCALS-Rex, *Atmos. Chem. Phys.*, 12, 355-369, doi: 10.5194/acp-12-355-2012, 2012.

Model	Domain Extent	Horizontal Resolution, inner region (lat x lon)	Vertical Levels (>700 hPa)	Forecast Frequency	Forecast Hours Analyzed	Aerosol Scheme	PBL Scheme	Land Emissions	Micro-physics	Aerosol-Cloud feedback	Investigators
CAM4	Global	1.9°x2.5°	26(6)	Daily	48-72	MOZART bulk (Lamarque et al. 2005)	Holtzlag Boville (1993)	see Appendix	1-moment	no	C. Hannay
CAM5	Global	1.9°x2.5°	30 (10)	Daily	48-72	MAM 3 modes	UW PBL	Lamarque et al. (2010)	2-moment Morrison	yes	C. Hannay
GFDL AM3	Global	2.0°x2.5°	48 (12)	Daily	24-48	2 or 3 modes (Donner et al. 2011)	Lock et al (2000)	Lamarque et al. (2010)	1-moment Rotstayn	yes	Y. Lin
ECMWF/MACC 36R1	Global	0.225°x0.225°	91 (21)	Daily	0-24	Sectional 8 bins Morcrette (2009)	eddy-diff mass-flux (Köhler et al 2011)	Morcrette et al. (2009)	1-moment bulk	No	J.-J. Morcrette
UKMO MetUM, G52	Global	0.375°x0.562°	70 (20)	Twice Daily	0-12	CLASSIC Bellouin et al. (2007)	Lock et al. (2000)	AeroCom-2	1-moment Wilson & Ballard	yes	J. Mulcahy
IARC iRAM 1.2	170W-40W 40S-40N	0.25°x0.25°	28 (12)	N/A	N/A	Prescribed	E-ε turbulence closure	N/A	2-moment Philipps	Aerosols affect clouds	A. Lauer Y. Wang
PNNL WRF-Chem 3.2.1	93W-63W 36S-11S	9km x 9km	64(48)	N/A	N/A	MOSAIC sectional 8 bins	YSU PBL	VOCA specified	2-moment Morrison	yes	Q. Yang W.I. Gustafson J. D.Fast
IOWA WRF-Chem 3.3	91W-65W 40S-12S	12km x 12km	74 (53)	N/A	N/A	MOSAIC Sectional 8 bins	MYNN 2.5	VOCA specified	2-moment Lin	yes	P. Saide S. Spak G. Carmichael
UW WRF-Chem 3.2.1	93W-64W 40S-7S	0.25°x0.25°	27 (15)	N/A	N/A	MADE/SORG AM 3 modes	UW PBL	VOCA specified	2-moment Lin	yes	R. George R. Wood

Table 1: Model parameters and physics.

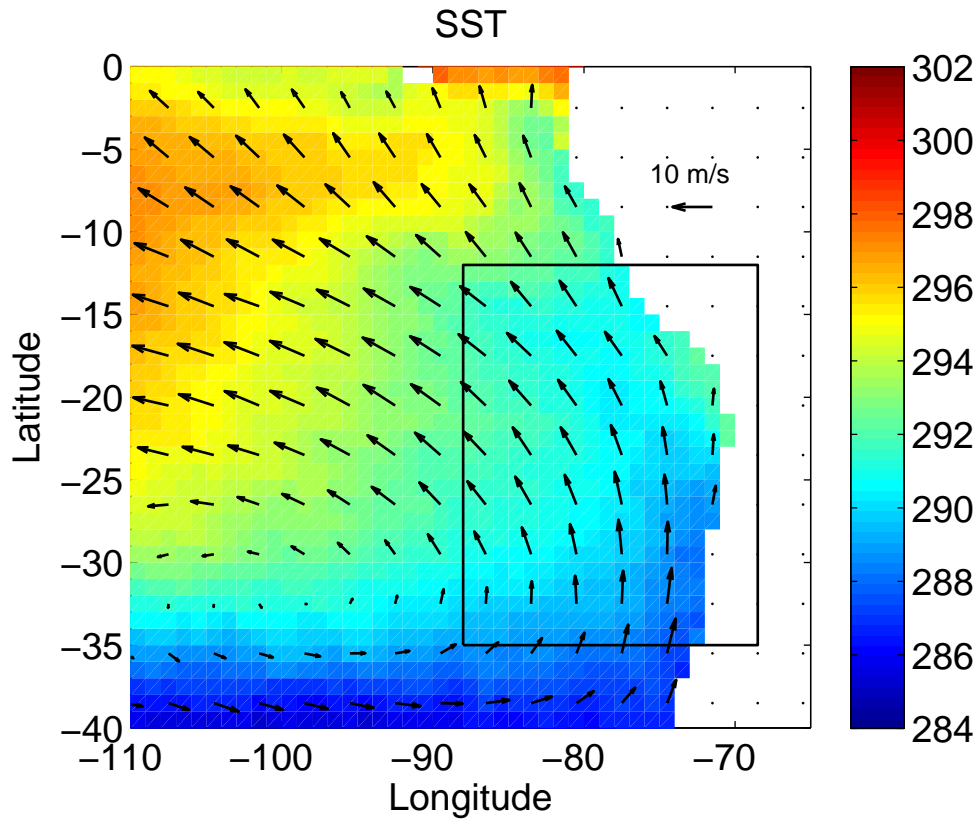


Fig.1. Observed SST (K) from AMSR-E and surface winds from QuikSCAT in the outer VOCA study region during the REx period, 15 Oct – 16 Nov 2008. The inner study region is shown as a black rectangle.

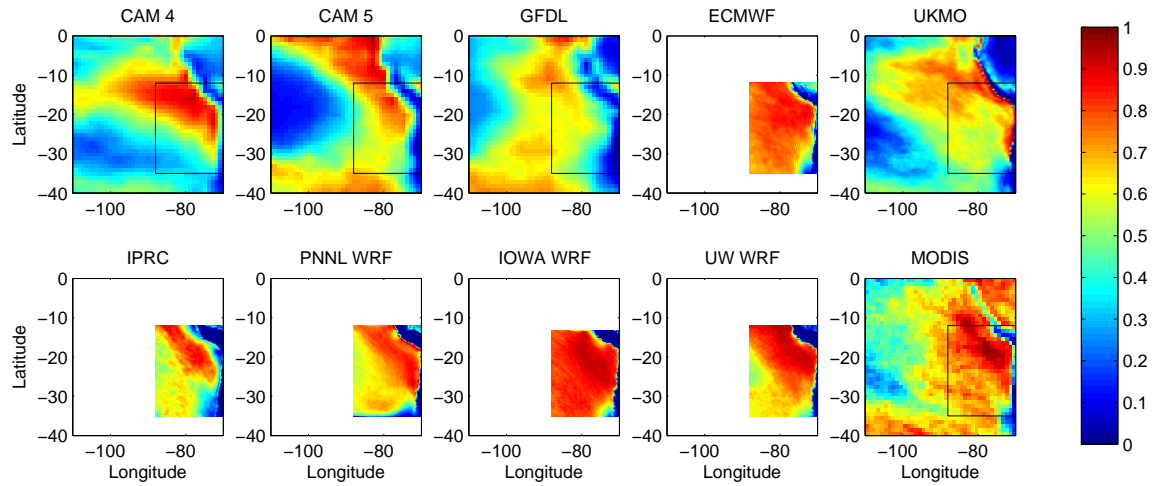


Fig. 2. Models' mean low cloud fraction at 10:30am local time (1530 UTC) compared with MODIS Terra daytime mean total cloud fraction. The extent of the inner VOCA study region is shown with a black rectangle.

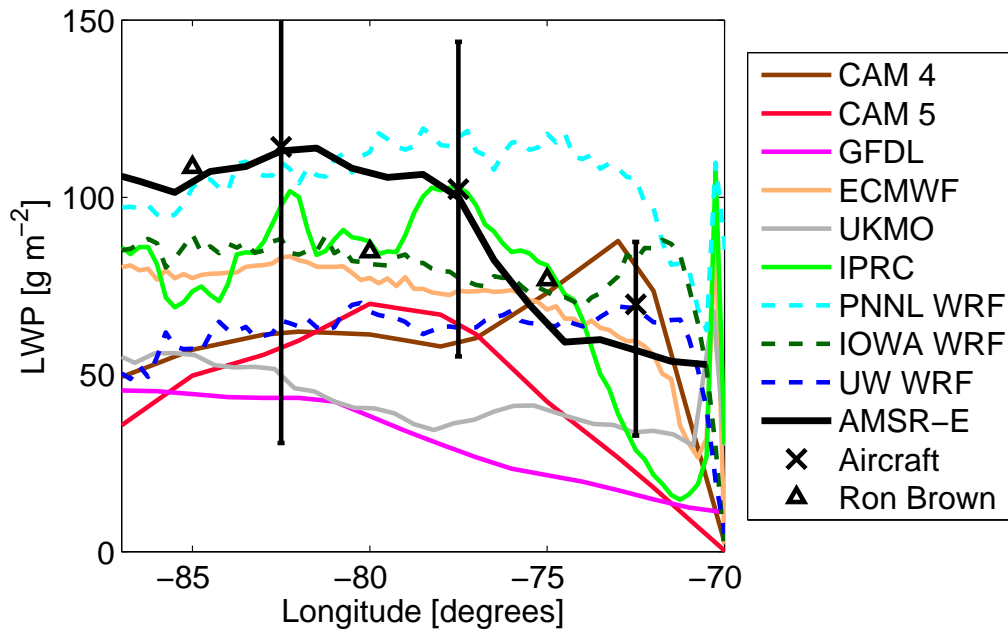


Fig. 3. Grid-box mean liquid water path (LWP) along 20°S compared with AMSR-E satellite mean of day and night passes and median LWP from microwave radiometer on the C-130 (Zuidema et al. 2012). Error bars represent interquartile ranges of aircraft leg-means. Also plotted as triangles are mean values measured by the Ron Brown from 2001-2008 (de Szoeké et al. 2012)

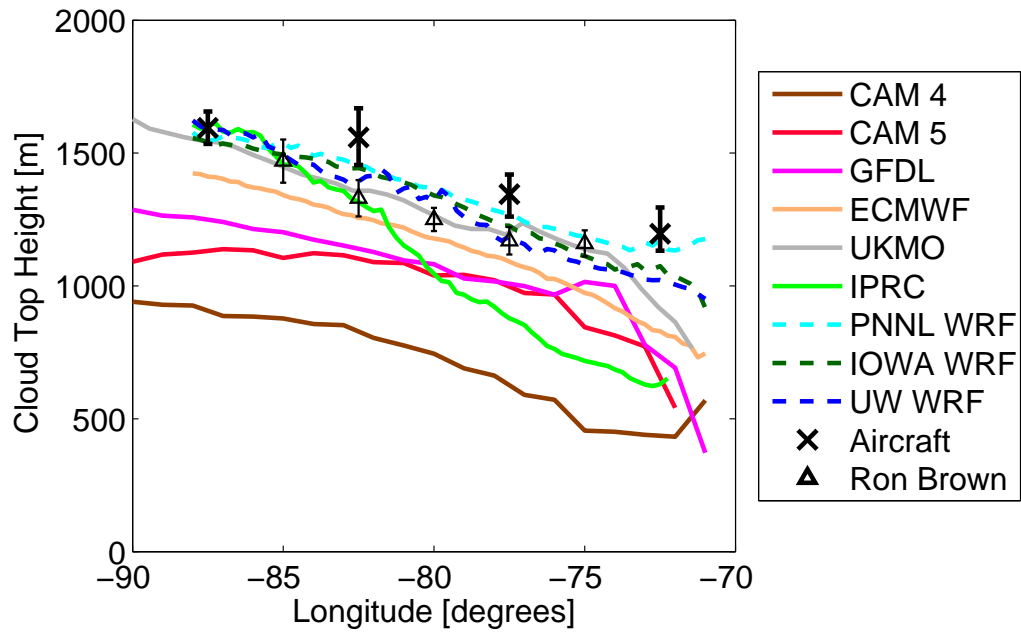


Fig. 4. Model-mean cloud-top height along 20° S compared with mean cloud-top measured using cloud radar from C-130 flights (Bretherton et al 2010). Mean observations from Ron Brown from 2001-2008 (de Szoeke et al. 2012) are plotted as triangles with bars as standard deviation.

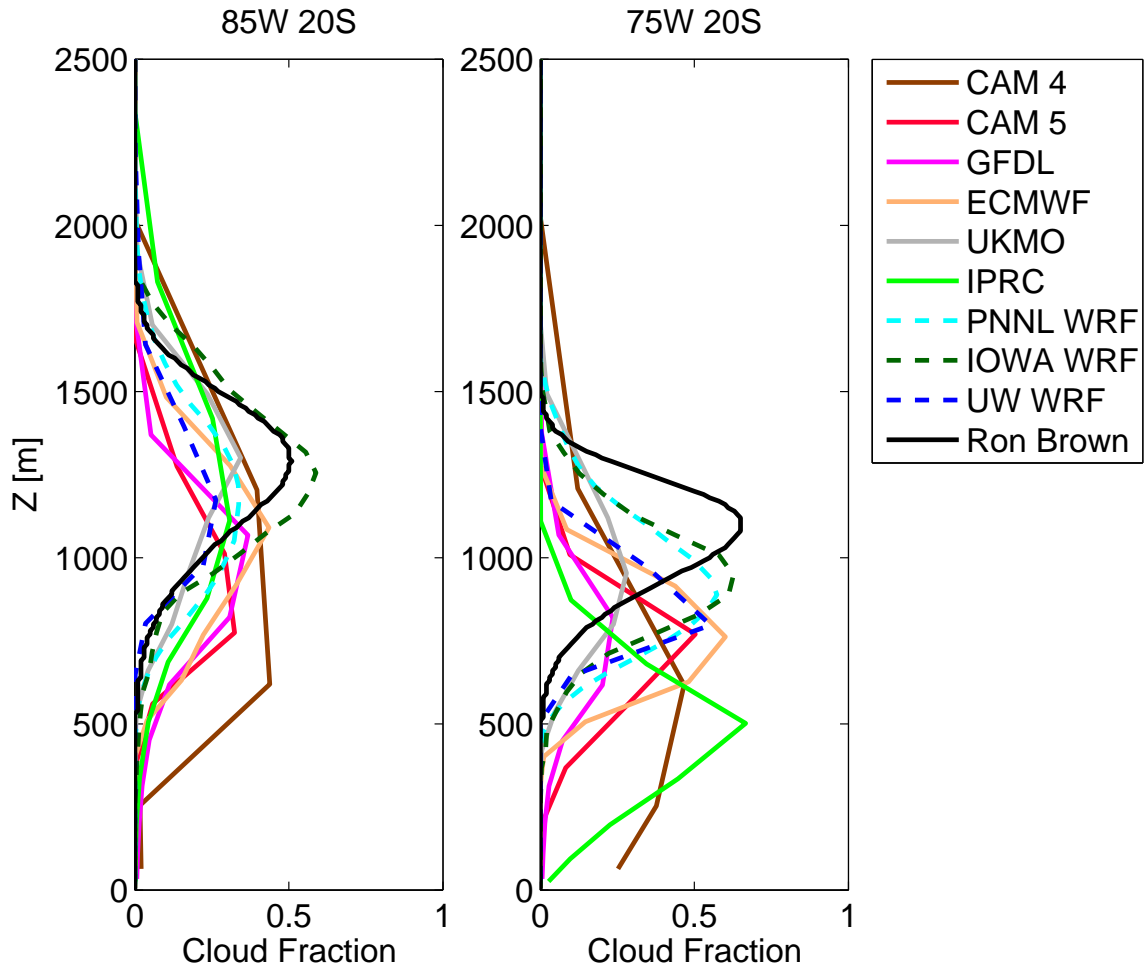


Fig. 5. Mean model cloud fraction at 85°W 20°S (left panel) and at 75°W 20°S (right panel). Also plotted is cloud fraction inferred from Ron Brown ship based measurements over nearby longitudes from Burleyson et al. (2013). See text for more details.

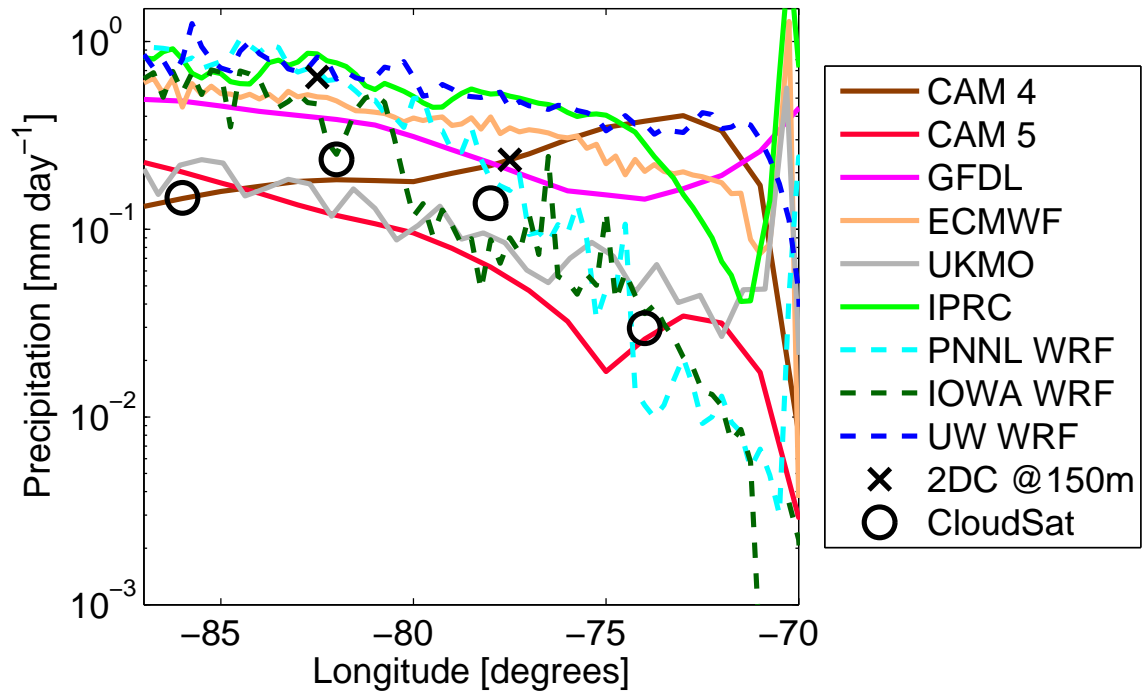


Fig. 6. Mean surface precipitation in mm day^{-1} along 20° S compared with leg-mean precipitation rate from C-130 estimates at 150m using a 2D-C probe, and with CloudSat climatology for Oct-Nov 2007-2010. The 2D-C precipitation mean for $70\text{-}75^\circ \text{ W}$ is less than $0.001 \text{ mm day}^{-1}$ and not shown.

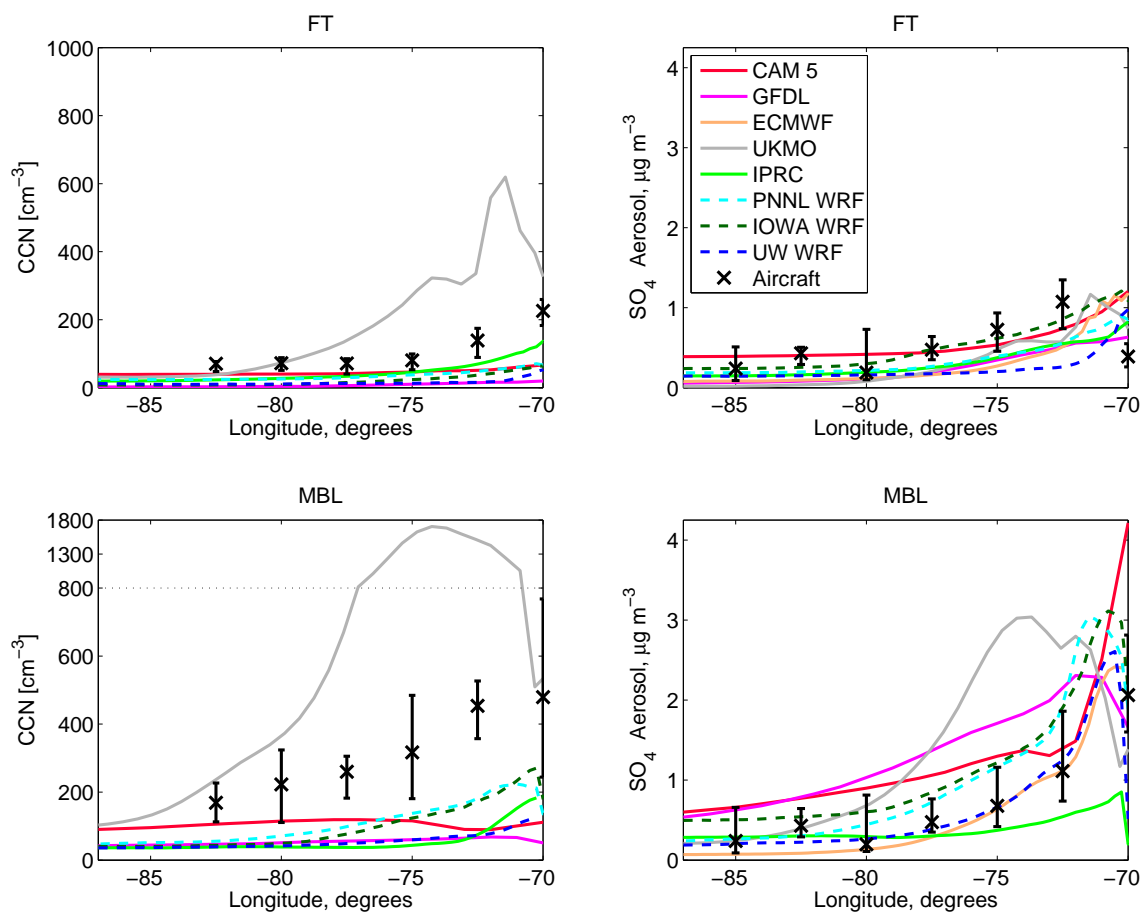


Fig. 7. CCN concentrations at 0.1% supersaturation in cm^{-3} along 20° S are shown in the left panels. Free tropospheric (FT) mean (top left) and concentration at 150m (lower left). C-130 nephelometer means are plotted with 'x' symbols. Sulfate aerosol (SO_4) dry mass concentrations in $\mu\text{g m}^{-3}$ of diameter range $0.05\mu\text{m} - 0.5\mu\text{m}$ measured with AMS (C-130 and BAe-146) are compared with model dry mass concentration along 20° S (see Allen et al. 2011) in the right panels for the FT (top right panel) and MBL mean (bottom right panel) The lower left plot is linearly rescaled at the top of the plot. The lower right panel is modified from a figure in Mechoso et al. (2014) to add aircraft sampling variability. Note that ECMWF CCN concentrations are unavailable.

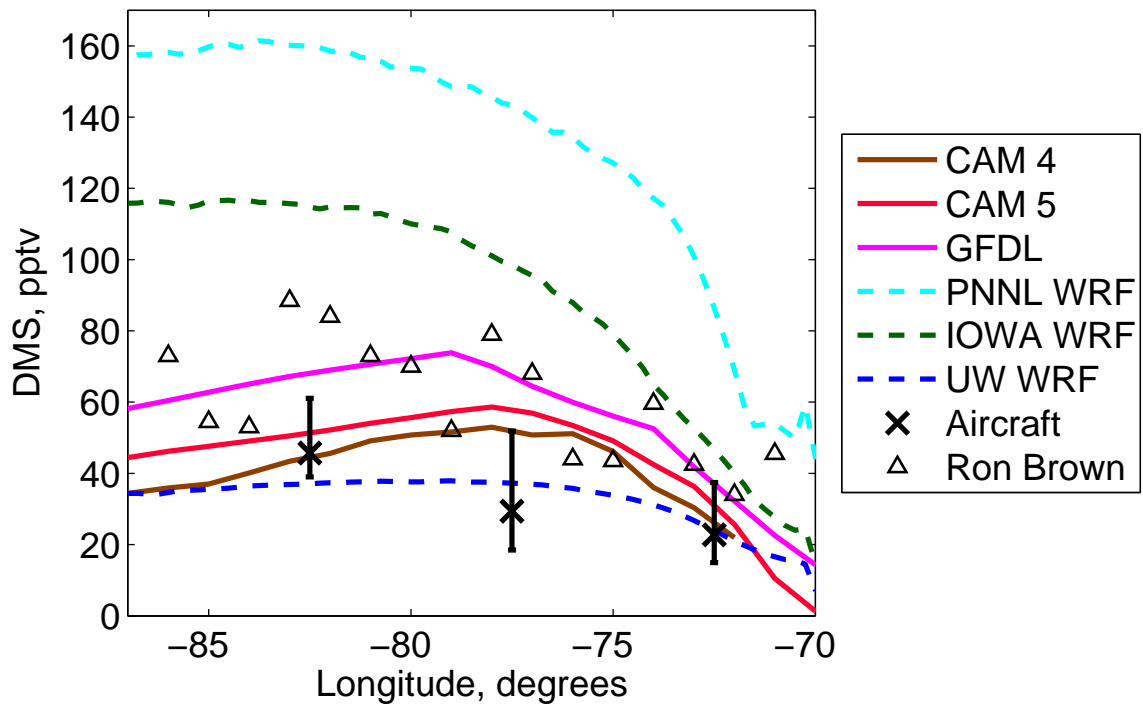


Fig. 8. MBL-mean DMS concentrations in pptv along 20°S for some models along with C-130 observed MBL-means marked by 'X'. Near-surface means from the Ron Brown ship-based measurements (M. Yang et al. 2011) are marked by triangles.

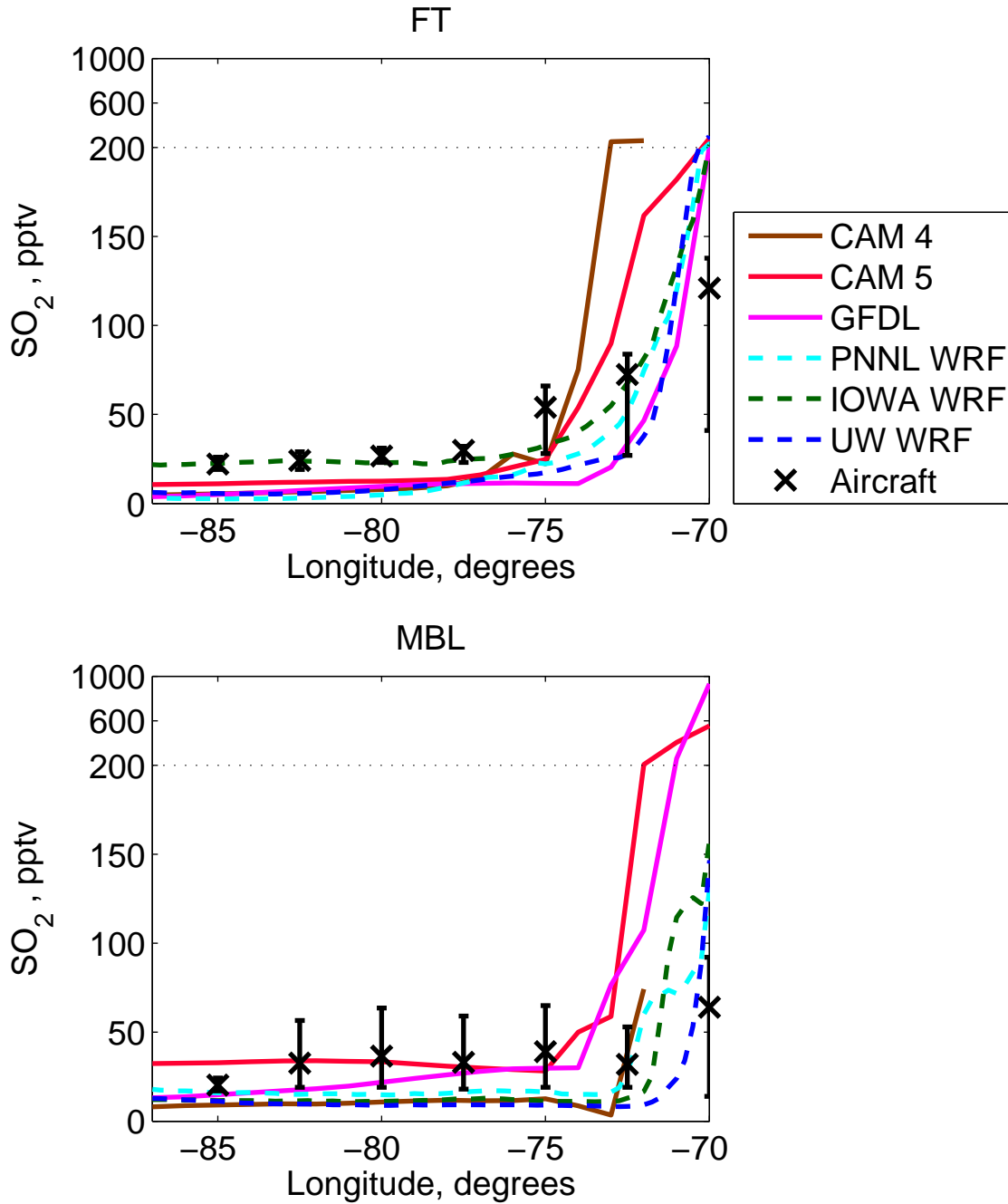


Fig. 9. Mean modeled SO₂ (gas) concentration along 20° S in pptv and C-130 aircraft means. The top sections of the both panels are rescaled.

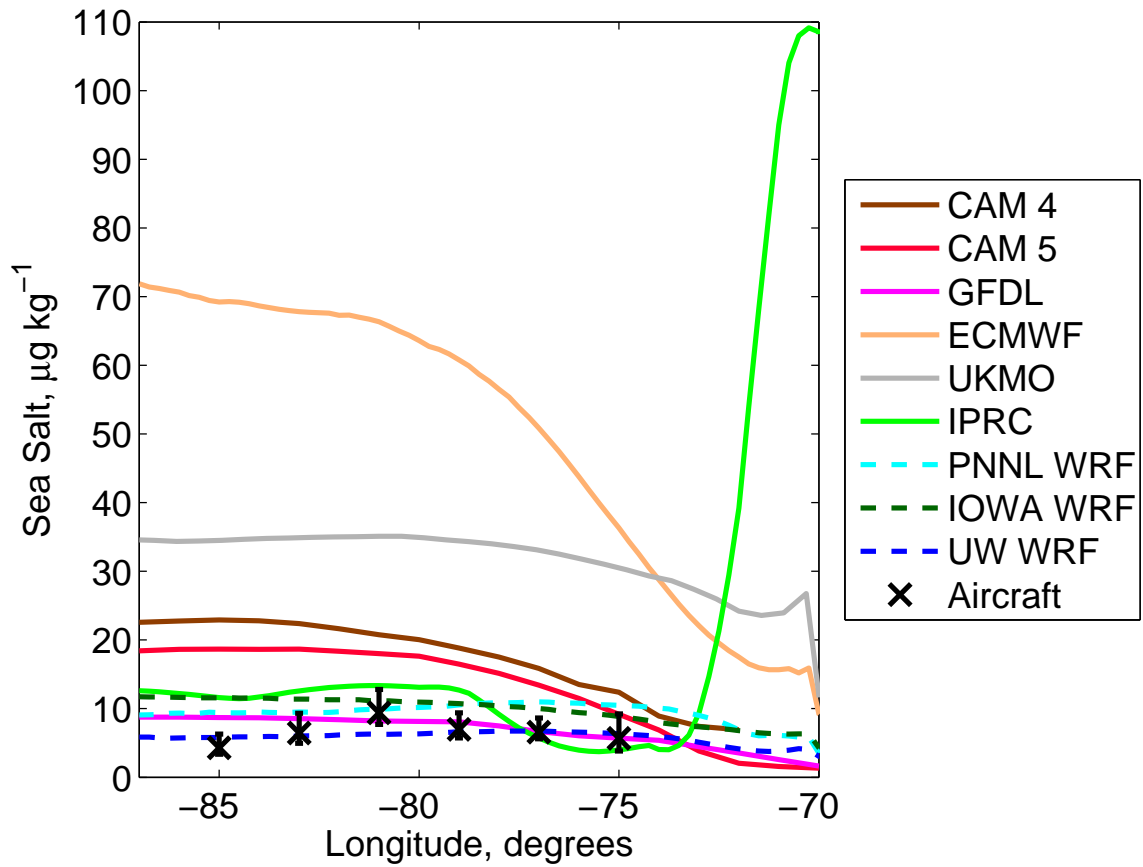


Fig. 10. Mean sea-salt aerosol dry mixing ratio along 20°S ($\mu\text{g kg}^{-1}$) compared with C-130 particle counter and Giant Nuclei Impactor measurements from Blot et al. (2013)

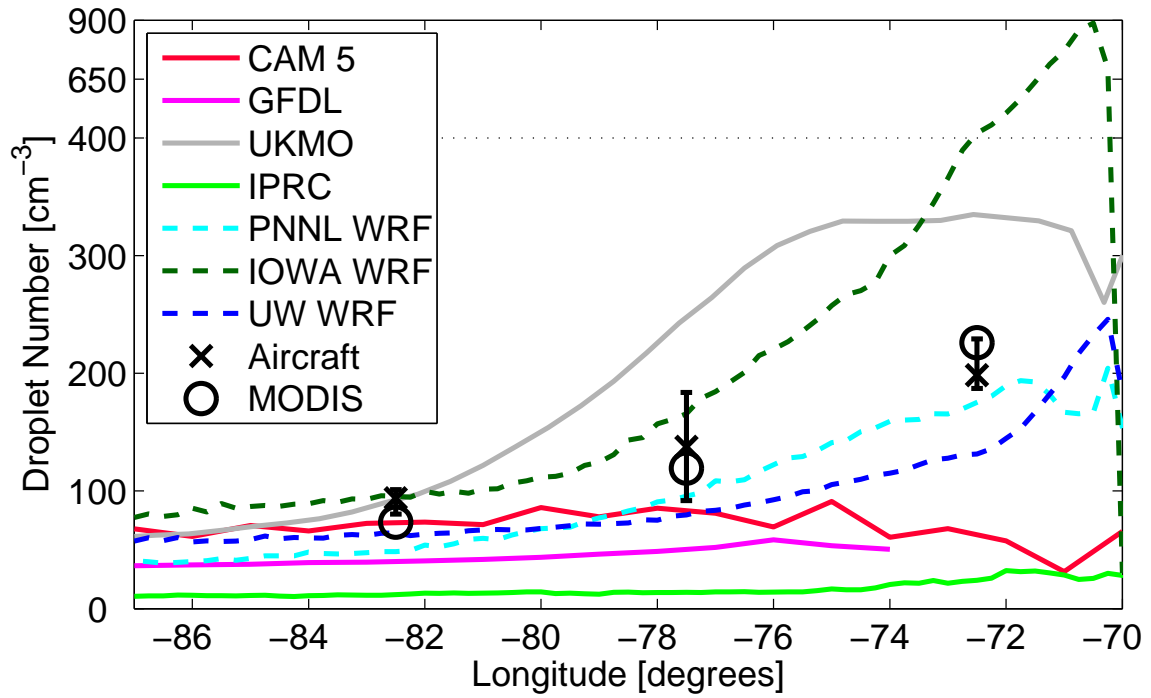


Fig. 11. Mean cloud droplet number concentration, N_d , in cm^{-3} along 20°S compared with mean C-130 measurements using a PMS cloud droplet probe and FSSP and also with MODIS estimates. This figure is modified from Mechoso et al. (2014) to add aircraft sampling variability and MODIS data. The top section of the plot is rescaled.

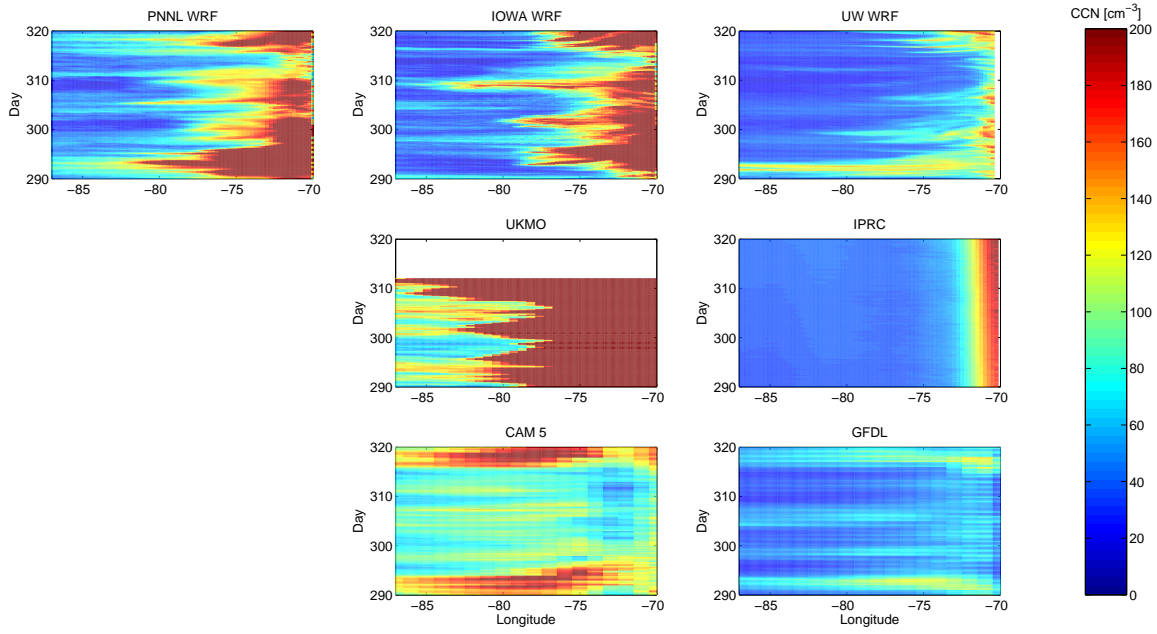


Fig. 12. Hovmöller diagrams of CCN at 0.1% supersaturation at 150m height along 20°S. CCN concentrations are given in cm^{-3} .

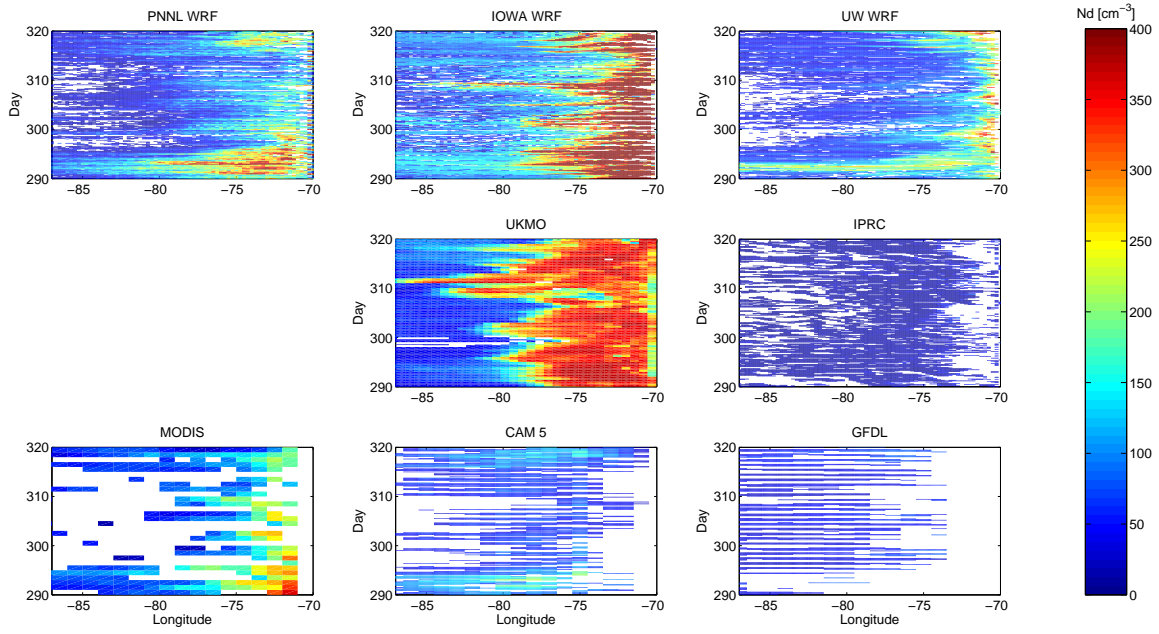


Fig. 13. Hovmöller diagrams of models' mean cloud droplet concentration, N_d , in cm^{-3} along 20°S . Daily mean MODIS estimates from Bretherton et al. (2010) are shown in the lower left.

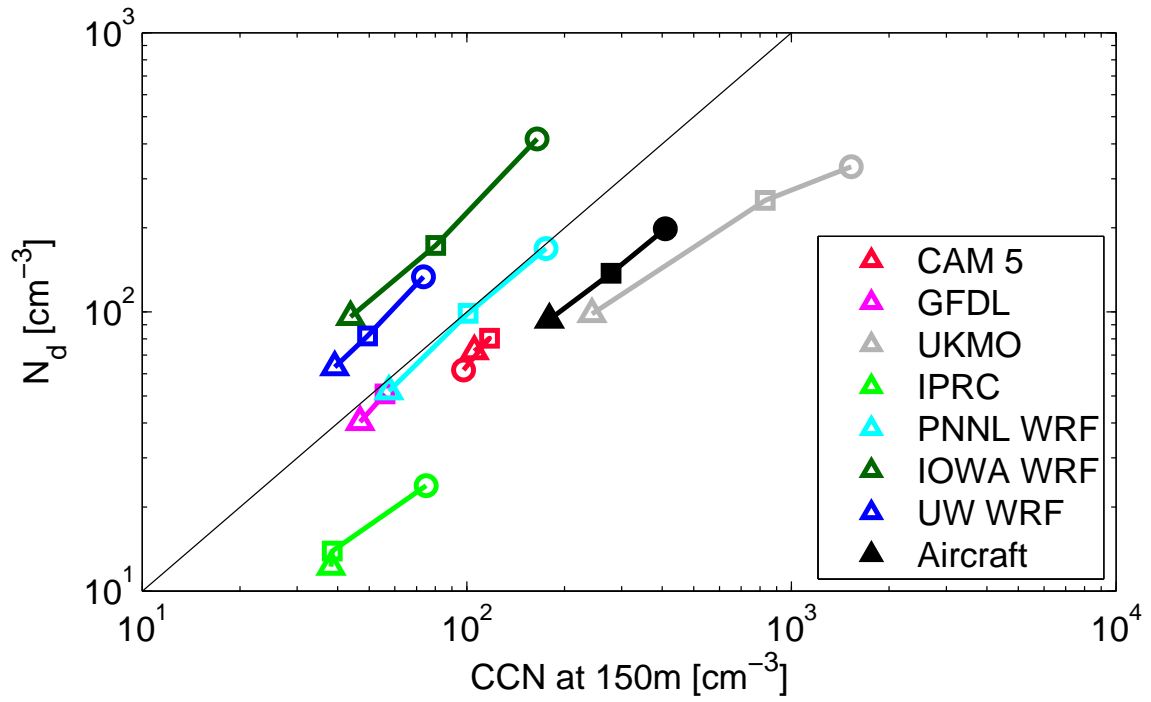


Figure 14. Mean cloud droplet concentration versus CCN (0.1% SS) at 150m for models and aircraft observations at 20°S. Values are binned from 80-85°W (triangles), 75-80°W (squares) and 71-75°W (circles). A one-to-one line is also plotted.

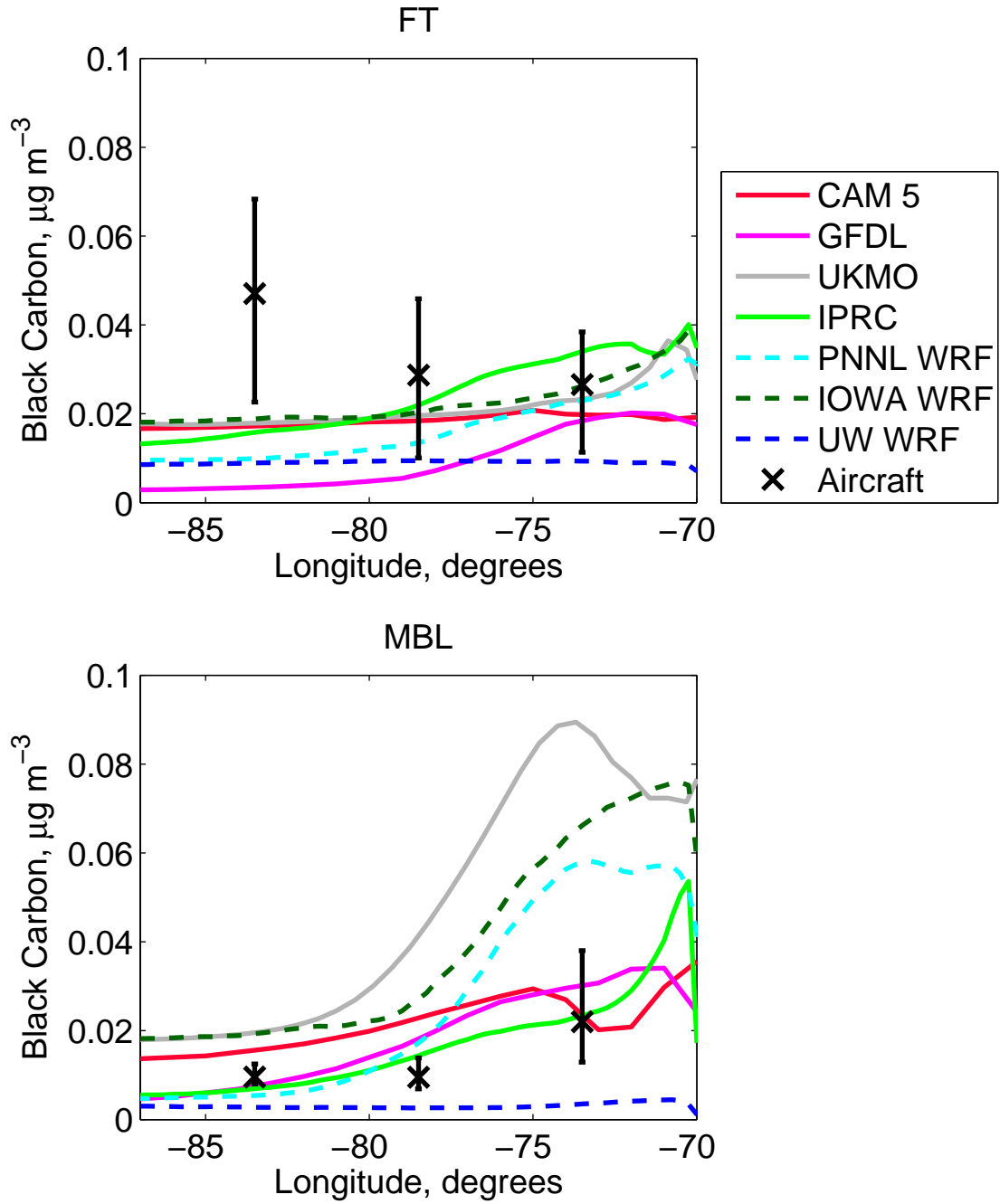


Fig.15. Total modeled black carbon aerosol mass concentration ($\mu\text{g m}^{-3}$) along 20° S compared with C-130 single-particle soot photometer measurements (diameters $0.087\text{-}0.4\mu\text{m}$).

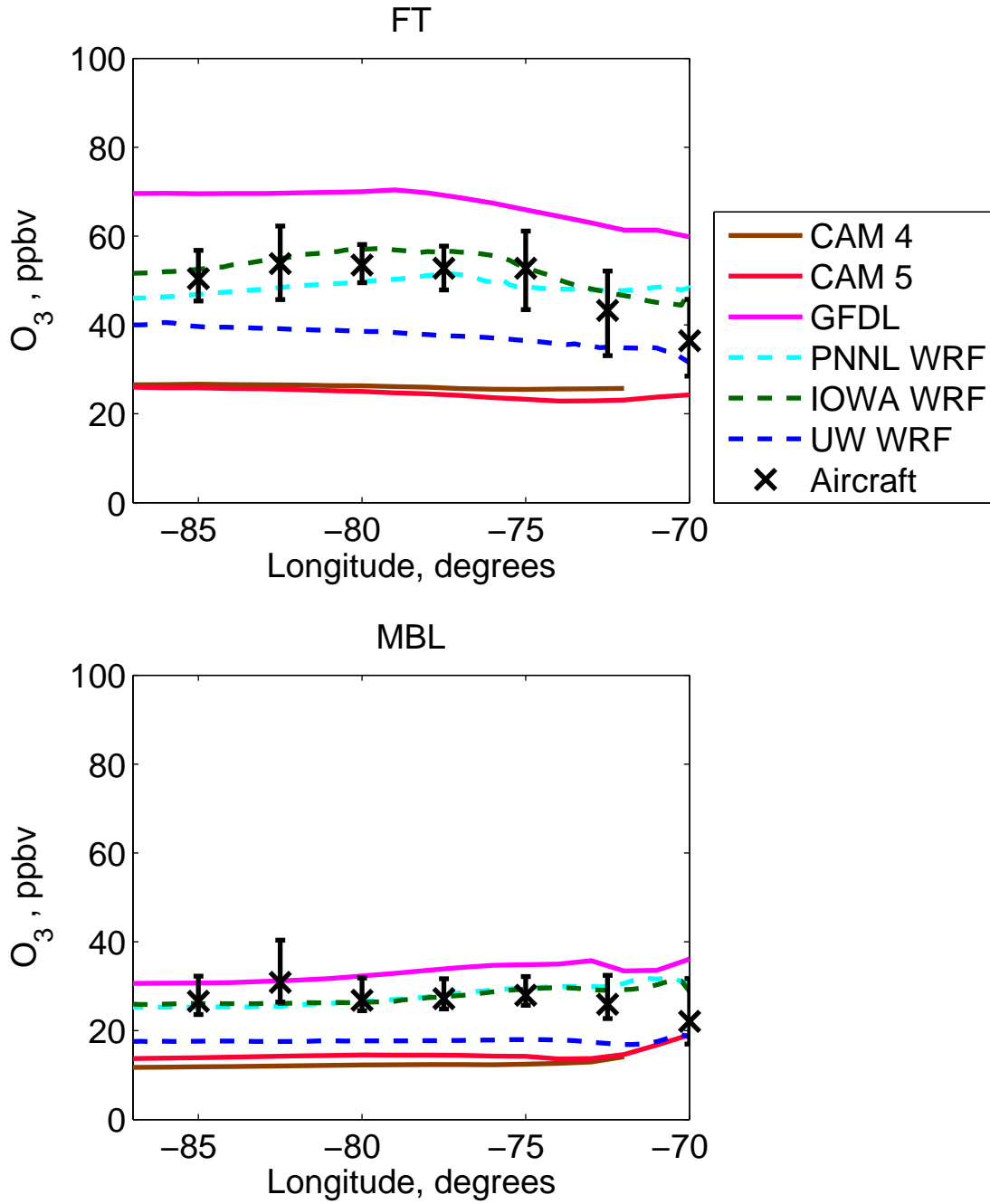


Fig. 16. Ozone concentration (ppbv) compared along 20° S with C-130 and BAe-146 aircraft observations.